COMPLEX MODULUS PREDICTION OF ASPHALT CONCRETE PAVEMENT CORES

A Thesis

by

MENG LING

Submitted to the Office of Graduate and Professional Studies of
Texas A&M University
in partial fulfillment of the requirements for the degree of

MASTER OF SCIENCE

Chair of Committee,	Robert L. Lytton
Committee Members,	Nasir G. Gharaibeh
	Paul Frederick. Dahm
Head of Department,	Robin Autenrieth

December 2013

Major Subject: Civil Engineering

ABSTRACT

Complex modulus is one of the key parameters in the Mechanistic-Empirical Pavement Design Guide (MEPDG). The purpose of this study is to implement an accurate and high-efficiency mechanical method to measure and calculate the complex modulus gradient of asphalt concrete cores in different field locations. Because field cores are different from the asphalt mixtures made and compacted in the lab, field cores should not be substituted by lab made lab compacted (LMLC) asphalt mixtures perfectly. For field cores complex modulus measuring methods, except some expensive pavement field testers, empirical and semiempirical models are widely used, but an accurate mechanical test method is more desired. In this research, Arizona, Yellowstone National Park and Texas field cores and three types of asphalt mixtures including hot mix asphalt (HMA), foaming warm mix asphalt (FWMA), and Evotherm warm mix asphalt (EWMA) were used. There were nearly forty field cores with different aging times from these three locations have been collected and tested using this new viscoelastic method. The complex modulus at a random depth and the depth of highly aged pavement can be calculated and estimated from these stiffness gradient figures. After analyzing the results, a strong correlation between test results and solar radiation and some other models have also been established which can be used for estimating the complex modulus of an in-service pavement.

DEDICATION

This thesis is dedicated to my parents, my mother Shaohong Huang and my father Tianqing Ling, who help and encourage me in my life.

ACKNOWLEDGEMENTS

I would like to take this opportunity to thank my committee chair Dr. Lytton and my committee members, Dr. Gharaibeh and Dr. Dahm, for their guidance and support throughout the course of this research.

Thanks also go to my friends and colleagues and the Department of Civil Engineering faculty and staff for making my time at Texas A&M University a great experience. I also want to extend my gratitude to Dr. Luo from Texas Transportation Institute for her involvement and help in this research and Dr. Glover from Department of Chemical Engineering for his funding support.

Finally, thanks to my family, especially my parents, for their continued love and support.

TABLE OF CONTENTS

Page

LIST OF FIGURES

Page

LIST OF TABLES

Page

1. INTRODUCTION

The study of pavement properties is an important topic for pavement researchers. Through these years, several methods have been used to evaluate and estimate pavement properties, one method is to run some tests on the Lab Mixed Lab Compacted (LMLC) specimens to mimic the real pavement, and the other method is running tests on field cores while the other current approach is based on empirical or semiempirical models. Unfortunately, for these models there are a number of kinds of asphalt binders and aggregates in asphalt mixtures like different kinds of warm mix asphalt (WMA) which increase the difficulties to establish a general relationship (Shu and Huang 2008). For this study, a mechanical test method was conducted and some relevant models were developed which are more conclusive and reasonable for measuring and estimating the modulus of most asphalt mixtures including both LMLC cores and field cores no matter what kinds of asphalt mixtures they are.

More than 90% of pavements are flexible pavements in the United States of America and 85% pavements in China are also flexible pavements, meanwhile more flexible pavements are planned or under construction. Complex modulus of flexible pavements is one of the most essential factors which affect pavement properties. The complex modulus which influences the structural response of flexible pavements has been used in many models and tests. The complex modulus has become a promising parameter to evaluate both the rutting and the fatigue cracking resistance of the asphalt mixtures. The complex modulus gradient of pavement is also a good indicator to show

how the pavement has been aged versus depth to see when it became more brittle and susceptible to cracking. Environmental factors like humidity and solar radiation and transportation factors like traffic load and traffic direction are not easily simulated in the lab, even with some tests and pavement conditions simulations like the Hamburg wheel track test and environmental rooms which are now in use. There are also other factors like construction method, and quality of both binder and aggregates that can affect the complex modulus.

Air voids of pavement and temperature of pavement are two of the well-known direct factors. X-ray computed tomography (CT) is an accurate method to measure air voids content and distribution versus depth. In this project, X- ray CT tests have been run on the Texas FM 973 field cores collected from the Warm Mix Asphalt Evotherm (EVO) section (see Figure 1), the Hot Mix Asphalt (HMA) section (see Figure 2) and the Foaming Warm Mix Asphalt (FWMA) section (see Figure 3) with different aging times. Unlike the LMLC specimens, the air voids distribution figures of field cores have shown nonuniform air void distribution, interconnected air voids are correlated with binder oxidation and hardening which indicate higher air voids would result in aging faster (Woo et al. 2008). From the X-ray CT results of field cores (see Table 1), the air voids vary through depth while the air voids of specimens compacted by Superpave gyratory followed a bathtub shape (Masad et al. 2002). The results show that the air voids are different even though these cores were collected from the same section of the same pavement. In the mean time, temperature is also one of the primary factors which affect the modulus of AC layers. According to related researches (Nazarian and Alvarado

2006), the temperature gradient also has a strong influence on the stiffness of AC pavements. Consequently, it is better to run tests on field cores instead of LMLC mixtures.

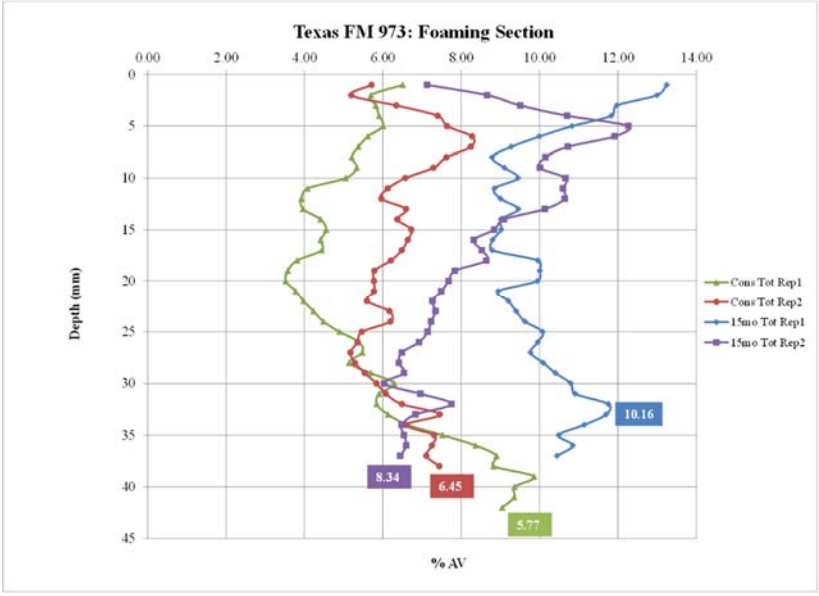

Figure 1. Air voids distribution of Evotherm section

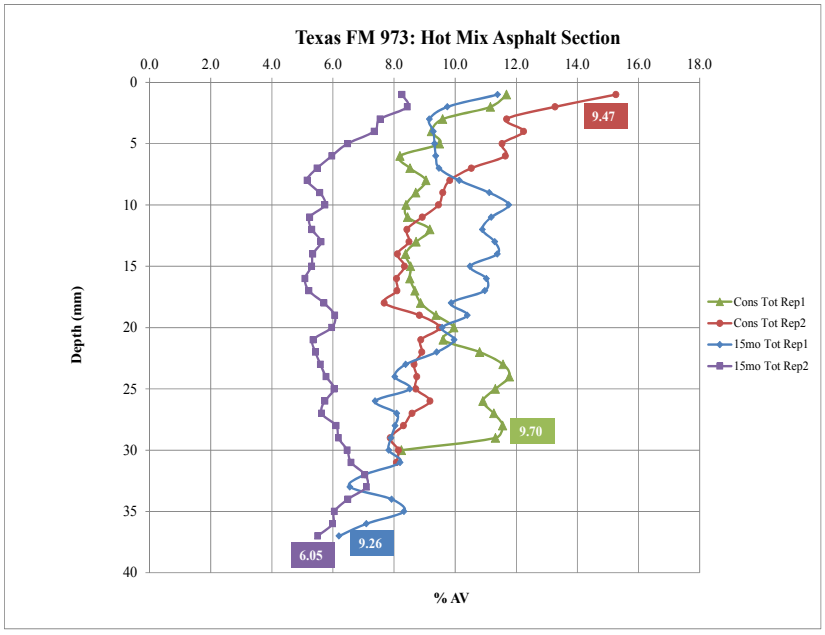

Figure 2. Air voids distribution of HMA section

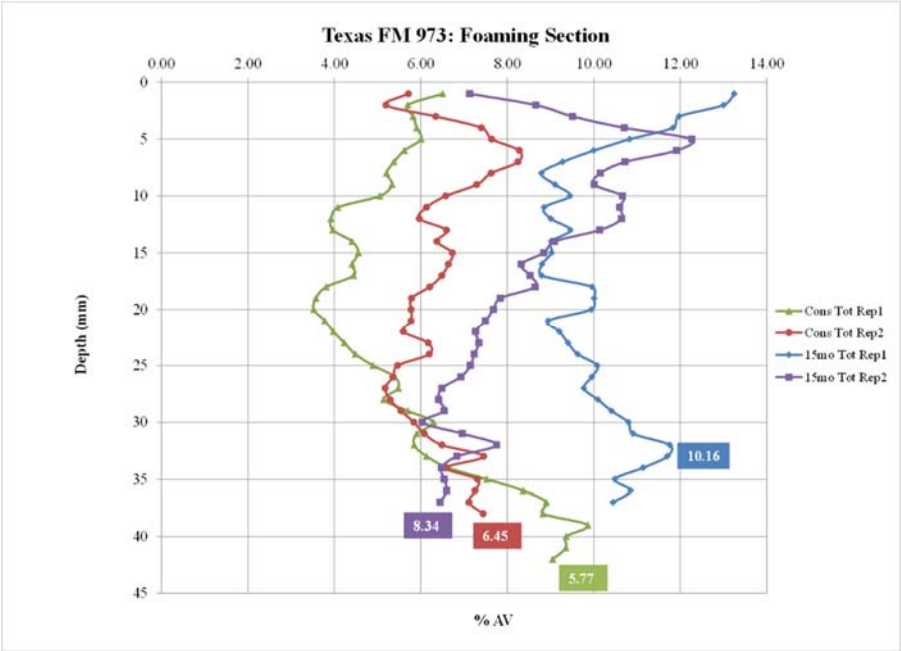

Figure 3. Air voids distribution of Foaming section

Table 1. Air voids distribution in three sections

Air Voids %	Replicate	HMA Section			Foaming Section			Evotherm Section		
		1 month Aged	15 months Aged	% Diff with Time	1 month Aged	15 months Aged	% Diff with Time	1 month Aged	14 months Aged	% Diff with Time
Total	1	9.7	9.26	20.10%	5.77	10.16	-51.40%	5.48	7.32	1.80%
	2	9.47	6.05		6.45	8.34		8.59	6.5	
Avg.		9.58	7.66		6.11	9.25		7.04	6.91	
Interconn-ected	1	5.94	5.32	51.80%	0	3.92	-322.20%	0.06	2.36	58.80%
	2	5.29	0.09		1.06	5.04		3.93	0.88	
Avg.		5.61	2.71		1.06	4.48		3.93	1.62	
% Diff Total vs. Interconnected		41.40%	64.70%		0.826	0.516		44.10%	76.60%	

The dynamic shear rheometer (DSR) test can be used for characterizing the viscoelastic behaviors of binders at medium to high temperatures or extracted from LMLC cores and field cores. For field cores, asphalt binders need to be extracted and recovered first, then the binders need to be run with the DSR. Trichloroethylene (TSE) which is widely used in this procedure is regarded as carcinogenic and environmentally hazardous which is not welcomed (Collins-Garcia et al. 2000; Tia and Choubane 2000). Meanwhile, extraction and recovery of asphalt binder may affect asphalt mixture properties which may change the properties of asphalt mixtures. What's more, this procedure only focuses on dynamic shear modulus of asphalt, not the dynamic modulus of asphalt mixture. There are also many empirical and semiempircal models which have been established to measure the modulus of pavement. However, tests have been

conducted (Birgisson et al. 2005) to evaluate the Witczak predictive modulus equation in Florida and the results showed there is a bias for mixtures common to Florida.

The Direct Tension Test (DT) which is introduced in this thesis can be used to directly measure the complex modulus of an asphalt mixture. The advantages of this DT test are saving time and money, more accurate to evaluate asphalt mixture, and no harm to people.

1.1. Research Objectives

The final objective of this thesis is to apply an accurate and rapid mechanical technique to measure and estimate the stiffness gradient of field aged asphalt mixtures in an in-service pavement. This test is a nondestructive test which can save limited field cores.

- Develop an efficient and accurate methodology to calculate the undamaged viscoelastic properties of field-aged asphalt concrete cores.
- Compare stiffness gradient with different asphalt mixtures types, aging times, and locations.
- Develop several models to estimate the complex modulus of local pavement.

1.2. Thesis Outline

This thesis is organized in five chapters as subsequently described. Chapter 1 includes introduction and research objectives. Chapter 2 presents a literature review of relevant papers and topics. Chapter 3 presents detailed information of this novel test including mechanical analysis and test procedures. Chapter 4 details some models derived from this test, and Chapter 5 contains conclusions, results, and future work.

2. LITERATURE REVIEW

This chapter includes a summary of important background information required to meet the research requirements and understand the limitations of current methods. First, an overview of the asphalt mixture fundamental properties and some relevant researches regarding the modulus of field aged asphalt mixtures are described in detail. Next, a few widely used applicable laboratory test methods to estimate the complex dynamic modulus of field aged asphalt mixtures are discussed. These test methods are outlined because they are often used to evaluate mixture properties. Simultaneously, some limitations associated with these current tests are highlighted.

2.1. Basic Knowledge of Asphalt Mixtures

Asphalt concrete is a composite material for pavement construction which contains asphalt binder and mineral aggregates including both course and fine aggregates. The asphalt binder is used as a binding material to glue aggregates together and the aggregates are used to be a stone framework to supply strength for asphalt mixtures. Asphalt binder displays temperature susceptibility, viscoelasticity and chemically organic properties. First, for temperature susceptibility, asphalt binder is stiffer when temperature is low while asphalt binder is softer when temperature is high. Temperature and loading rate can be used interchangeably which means a slow loading rate equals high temperature whereas high loading rate equals low temperature. Second, asphalt binder also displays both viscous and elastic characteristics, when it is at high

temperature, it behaves as a viscous fluid while at low temperature it behaves as an elastic solid. Third, asphalt is easily oxidized which would cause cracking in the asphalt mixture.

There are many kinds of mineral aggregates which can be used like limestone and quartz stone. The aggregate material need to provide enough shear strength to resist repeated load. Cubical, rough-texture aggregate is better than rounded, smooth-textured aggregates because rounded aggregates cannot provide as much resistance nor hold the aggregate together more tightly. For the asphalt mixtures, its behavior should be analyzed by considering asphalt binder and aggregates together. In pavement engineering, there are three primary pavement distresses: permanent deformation (see Figure 4), fatigue cracking (see Figure 5), and low temperature cracking (see Figure 6).

Figure 4. Permanent deformation

Figure 5. Fatigue cracking

Figure 6. Low temperature cracking

2.2. Effect Factors of Modulus of Field Aged Cores

The complex dynamic modulus is one of the most essential properties of asphalt concrete. There are two main factors which affect the magnitude of modulus. The first one is temperature and the second one is aging and oxidation (Huang and Grimes 2010). The research by Nazarian and Alvarado (2006) shows that temperature gradient is one of the factors which can affect dynamic complex modulus. In order to develop the modulus-temperature relationship, a portable pavement analyzer was used to measure this in south Texas. The variation in modulus with temperatures changes like a circle because the modulus is high when the temperature is low while the modulus is low while the temperature is high. Some observations have been made after the tests. At a given temperature, the difference of modulus between the cooling and heating cycles in this test is less pronounced when the maximum test temperature is smaller. Second, the modulus-temperature relationship is independent of the maximum temperature for the heating cycles but it changes for the cooling cycles. Low temperature cracking is one of the most popular pavement distresses in cold weather climates and permanent deformation (rutting) is the most prevalent distress in hot weather climates.

Another factor which could impact complex modulus of asphalt concrete is oxidation. Binder oxidation happens once mixing and compacting starts, and it continues being aged in field. When binder is oxidized, asphalt binder becomes stiffer and asphalt mixtures become more susceptible to fatigue cracking and thermal cracking. Recent researches have indicated that binder can be aged deeply into pavement. Result of a

research conducted by Woo et al. (2008) indicates that there is a direct relation between pavement aging and interconnected air voids.

In the research, field cores were collected from three Strategic Highway Research Program long-term pavement performance (LTPP) pavements in Texas. After collection, binder properties were measured after extraction and recovery. Then the total air voids and accessible air voids measurements were made. Cores were sliced into a 0.5 inch unit disks, air voids measurement and extraction and recovery were implemented with each slice. Two air voids measurement methods (SSD method and core lock method) were also used to compare the difference between these two methods and determine which method is more applicable for certain asphalt mixtures. The results showed that the SSD method had the better result when specimens had more uneven textures while the core lock method was better when specimens had bigger open holes. Thorough extraction and recovery were conducted to make sure solvent removal which can be confirmed with the size exclusion chromatography (SEC), and when there are more aged binders, the longer recovery time this procedure requires (Burr et al. 1993).

The DSR function $|G^*|$ equals G' divided by the ratio of η' to G'. The results show that a smaller DSR function which indicates a less aged binder that has a higher calculated ductility and appears to the lower right on the DSR map.

Several conclusions have been made after obtaining the results. One was that smaller accessible air voids can reduce the rates of binder hardening and aging. The second one was that the difference of aging between the top layer and other layers is not

as large as expected and it is dominated by the accessible air voids. And the third one was that the chip seal and overlay can reduce the binder aging.

Measured complex modulus and predicted complex modulus from Witczak predictive modulus equation were compared by Birgisson et al. (2005). Near thirty mixtures divided into two groups were used in this project, one was the laboratory-based mixtures and other was proven field performance mixtures.

The prediction model developed by Witczak is presented below:

$$\log\left|E^*\right| = -1.249937 + 0.029232\times\left(p_{200}\right) - 0.001767\times\left(p_{200}\right)^2 - 0.002841\times\left(p_4\right)$$
$$-0.058097\times\left(V_a\right) - \frac{0.802208\left(V_{beff}\right)}{V_{beff}+V_a} + \frac{\left[\begin{array}{l} 3871977 - 0.0021\left(p_4\right) + 0.003958\left(p_{3/8}\right) - \\ 0.000017\left(p_{3/8}\right)^2 + 0.005470\left(p_{3/4}\right) \end{array}\right]}{1+e^{\left[-0.603313-0.313351\times\log(f)-0.393532\times\log(\eta)\right]}} \quad (1)$$

This model was created using an extensive data base including 7400 points from 346 different mixtures. Aggregate properties, volumetric properties, loading frequencies, binder viscosity are related in this model (Bari and Witczak 2007).

In this equation, the input binder viscosity was obtained from three methods, first way to get it was the results of the Brookfield rotational viscometer test after short-term rotational thin film oven (RTFO) aged specimens, the second one was from the DSR after the RTFO test, the viscosity was calculated from an equation which is related to the phase angle and the complex shear modulus from the DSR test, and the third one was from recommended viscosity values by Fonseca and Witczak (1996). For the Brookfield rotational viscometer, tests were conducted at three temperatures, and the DSR tests were conducted at two temperatures.

Comparisons have been made between predicted complex modulus and measured complex modulus for three temperatures. The results showed that the results for the viscosity value from the Brookfield rotational viscometer have the lowest bias and the highest R^2 value which are similar to the recommended values suggested by Fonseca and Witczak (1996). The results from the DSR test have the lowest R^2 values and the measured dynamic modulus are lower than the predicted ones.

2.3. Review of Current Standard Tests and Methods

One of the current standard tests to measure complex shear modulus is the DSR test (see Figure 7 and Figure 8). The DSR test is used to determine the viscoelastic properties of unaged and aged performance graded (PG) asphalt binders at intermediate to high temperatures. Based on Superpave methodology, the purpose of the DSR test is to measure the complex shear modulus (G*) and phase angle (δ) at a certain temperature. Asphalt is a viscoelastic material and G* consists of an elastic part and a viscous part. At higher temperatures, asphalts always have more viscous properties while at lower temperatures they usually behave like elastic solids. δ is the angle which shows the relation between elastic behavior and viscous behavior. The time lag between the applied shear stress and resulting shear strain or applied shear strain and resulting shear stress is related to the phase angle (δ).

For field cores, asphalt binders have to be extracted and recovered first, then the binders can be run with DSR. Trichloroethylene (TSE) which is currently widely used in

this procedure has been confirmed as a carcinogenic and environmentally hazardous chemical. Meanwhile, extraction and recovery of asphalt binder may affect asphalt mixture properties which would change properties of asphalt mixtures. What's more, this procedure only works on complex shear modulus of asphalt, not the dynamic modulus of asphalt mixture, but the direct tension test (DT) methodology which is recommended in this thesis can be used to directly measure the complex modulus of an asphalt mixture. The DT test is supposed to save time and money, be more accurate to evaluate asphalt mixture, and does no harm to people.

Figure 7. Dynamic shear rheometer

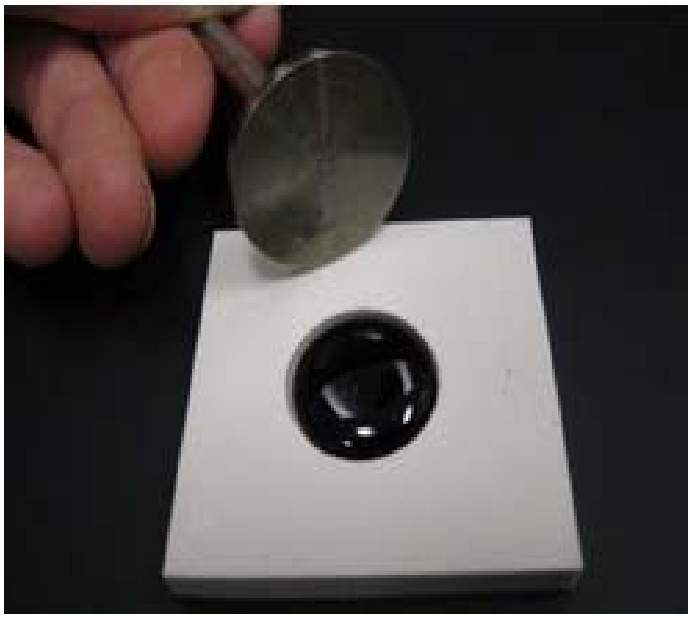

Figure 8. DSR samples

When tested at low temperatures, DSR test is not applicable so bending beam rheometer (BBR) was developed (see Figure 9). The BBR test is used to measure how much a binder deflects under a constant load at a constant test low temperature. Beam theory is used in the BBR test to calculate the stiffness of the asphalt beam sample. Some fluids like methanol, ethanol have been used in this test to prevent the water being frozen and the test temperature can be as low as 36˚C.

Figure 9. Bending beam rheometer

The Hirsch model is based on the law of mixtures which is a semi-empirical method for measuring developed by Hirsch in the 1960s. The final model which was constructed by Christensen (2003) is presented below:

$$|E^*|_{mix} = Pc\left[42000000 \times (1 - \frac{VMA}{100}) + 3 \times |G^*|_{binder}\left(\frac{VFA \times VMA}{10000}\right)\right] + (1 - Pc) \times \left[\frac{1 - VMA}{42000000} + \frac{VMA}{3 \times VFA \times |G^*|_{binder}}\right]^{-1} \quad (2)$$

$$Pc = \frac{\left(20 + \frac{VFA \times 3 \times |G^*|_{binder}}{VMA}\right)^{0.58}}{650 + \left(\frac{VFA \times 3 \times |G^*|_{binder}}{VMA}\right)^{0.58}}$$

where *VFM* = voids filled with mastic, *Pc* = aggregate contact volume fraction,

VMA= voids in mineral aggregate, *VFA*= volume of voids filled by asphalt volume of voids filled by asphalt.

In the Hirsch Model, the modulus is assumed to be three times larger than the binder shear modulus (Christensen et al. 2003; Dongre et al. 2005). Although the assumption provides high accuracy in many predictions, errors are still large because it is still missing some factors like the Recycled Asphalt Shingles (RAS) content and aggregate stiffness. From the research conducted by researchers at Iowa State University show that the Hirsch Model overestimates the modulus at high temperatures for Iowa mixes and underestimates the modulus for Minnesota mixes.

The Global Aging System (GAS) is another model which was calibrated from 40 field projects to evaluate asphalt viscosity (Fonseca and Witczak 1996). This model describes the temperature susceptibility of binders as the slope of the log log viscosity of binders versus the log test temperature which is shown below.

$$\log\log\eta = A + VTS\log T_R \tag{3}$$

where η is the viscosity of binders, T_R is the test temperature, and A and VTS are regression parameters.

There are two additional models which are applied for short-term aging and long-term aging.

$$\log\log\left(\eta_{t=0}\right) = a_0 + a_1\log\log\left(\eta_{orig}\right) \tag{4}$$

$$a_0 = 0.054405 + 0.004082\times code \tag{5}$$

$$\log(\log(\eta_{\eta>0})) = \frac{\log(\log(\eta_{\eta=0})) + A \cdot t}{1 + B \cdot t} \quad (6)$$

where $\eta_{t=0}$ is the lay-down viscosity of binders, η_{orig} is the original viscosity of binders, and the code is the binders hardening resistance.

According to Arizona validation site study by Western Research Institute (WRI), the GAS significantly assumes that the viscosity changes less than the actual condition especially for the top 13mm. Mirza and Witczak (1995) indicated that it is not considered applicable if the pavements are polymer modified asphalt pavements, Class "W" (waxy) or Class "B" (blown) asphalt pavements and open graded friction course (OGFC) asphalt pavements. Recent studies recommend that the long-term model should need some adjustment, and this model doesn't consider the binder properties. As a result, the GAS model has many limitations which should be modified. However, after analyzing the results of the DT test, the complex modulus of any type of asphalt mixtures can be used in the GAS model (Farrar et al. 2006).

3. ESTIMATION OF COMPLEX MODULUS GRADIENT OF FIELD-AGED CORES

Complex modulus is a required input value in the American Association of State Highway and Transportation Officials (AASHTO) design guide and the 2002 Minnesota Department of Transportation Design Guide for calculating permanent deformation, cracking damage, stress and strain (clyne et al. 2004; Shu and Huang 2008; El-Badawy et al. 2011; Dongre et al. 2005). There are some methods and models such as the Witczak model and the Hirsch model as stated previously, but a mechanical method is more desirable to measure the complex modulus of field cores because the empirical relationships can only give good estimates under conditions where they are developed. As a result, it is necessary to calculate the modulus and stiffness gradient with a mechanical method. Stiffness gradient shows that the highest modulus is at the top of the layer whereas the lowest modulus is on the bottom of the layer, and between these two levels there is a smooth curve connecting the two moduli (Koohi et al. 2012).

In this research, a nondestructive test was carried out to protect the specimens from being damaged. The specimens are rectangular with specific lengths, widths and varied thicknesses which depend on the pavement condition. Two test temperatures were included in this test to measure the relationship between temperature and complex modulus. And three field locations were also included in this test to confirm its applicability.

The results of this test are able to show the stiffness gradient of each field core, and it is easy to get the complex modulus of any thickness of core specimen. From these figures, it is interesting to know the depth of the highly aged surface of the pavement. Finally the results can be used in different programs and models to better evaluate pavement performance and estimate the future status of the pavement. After the test, some relevant models can be built to make this theory more practical and meaningful.

3.1. Material Preparation

Materials were taken from three places: Yellowstone National Park (Table 2), Arizona (Table 3), and Texas FM 973 (Table 4). Information regarding these cores is listed below:

Table 2. Arizona field cores information

Sample ID	Air Voids (%)	Thickness (Inches)	Aging Time (Months)
AZ1-1A	6.28	2	108
AZ 1-2A	7.15	2	108
AZ 1-3A	6.88	2	108
AZ 1-4A	8.08	2	108
AZ 1-1B	9.19	2	108
AZ 1-2B	7.28	2	108
AZ 1-3B	8.46	2	108
AZ 1-4B	8.08	2	108

Table 3. Yellowstone National Park field cores information

Sample ID	Air Voids (%)	Thickness (Inches)	Aging Time (Months)
1-3B-TOP-WP	6.83	2	48
1-3B-TOP-S	12.19	2	48
1-3B-BOT-WP	7.35	2	48
1-3B-BOT-S	11.94	2	48

Table 3 (*Continued*)

Sample ID	Air Voids (%)	Thickness (Inches)	Aging Time (Months)
1-2B-TOP-WP	5.48	2	48
1-2B-TOP-S	11.98	2	48
1-2B-BOT-WP	4.56	2	48
1-2B-BOT-S	9.07	2	48

Table 4. Texas FM 973 field cores information

Sample ID	Air Voids (%)	Thickness (Inches)	Aging Time (Months)
1-13-1	9.28	1	1
1-20-1	7.41	1.5	1
1-26-1	9.99	1	1
1-27-1	8.63	1	1
1-28-1	8.44	1	1
S1-2	6.64	1.5	9
S1-13	10.12	1	9
S1-20-1	11.09	1.5	9
S1-24	10.43	1	9
7-5-1	10.59	1.5	0
7-15-1	7.10	1.5	0
7-16-1	5.01	1.5	0
7-21-1	5.65	1.5	0
7-24-1	6.89	1.5	0
S7-5	7.33	1.5	8
S7-12	7.00	1.5	8
S7-15	9.03	1	8
S7-16	10.82	1.5	8
8-4-1	10.10	1.5	0
8-8-1	9.74	1	0
8-12-1	9.59	1.5	0
8-18-1	10.02	1.5	0
8-20-1	9.46	1	0
8-24-1	8.20	1.5	0
S8-4	9.22	1	8
S8-8	9.06	1	8
S8-12	7.74	1.5	8
S8-18	8.33	1.5	8

The cores of different aging times and collecting locations are prepared for this project in order to determine the eligibility of this methodology and try to build some general models. Once these cores were collected from the field, they were transferred to Texas A&M Transportation Institute McNew Laboratory (see Figure 10 and Figure 11).

Figure 10. Field cores collected from pavement (triple layers)

Figure 11. Field core collected from pavement (single layer)

The specimens are cut into rectangular sizes after cutting from cylindrical field cores as shown in Figure 12. Each specimen is 4 inches length and 3 inches width while the thickness varies between 1 inch and 2 inches.

Figure 12. Field core after cutting and trimming

Two steel end caps are glued using liquid epoxy on each end of the specimen as shown in Figure 13. When tested, one end cap is fixed at the bottom of the MTS machine with a ball joint, and the upper end is screwed to the dowel steel of the MTS machine to make sure the specimen can be easily pulled up in the chamber vertically without resistance. A gluing jig is used to ensure that the specimen was firmly glued and perfectly aligned.

Figure 13. Specimen with two end caps

The specimen glued with two center-aligned steel end caps should be put in the center of this gluing jig as shown in Figure 14. It takes half a day for the specimen with end caps with this gluing jig until the glue is completely set. There is a need to be careful to align the specimen to avoid any unwanted oscillations and moment in the test.

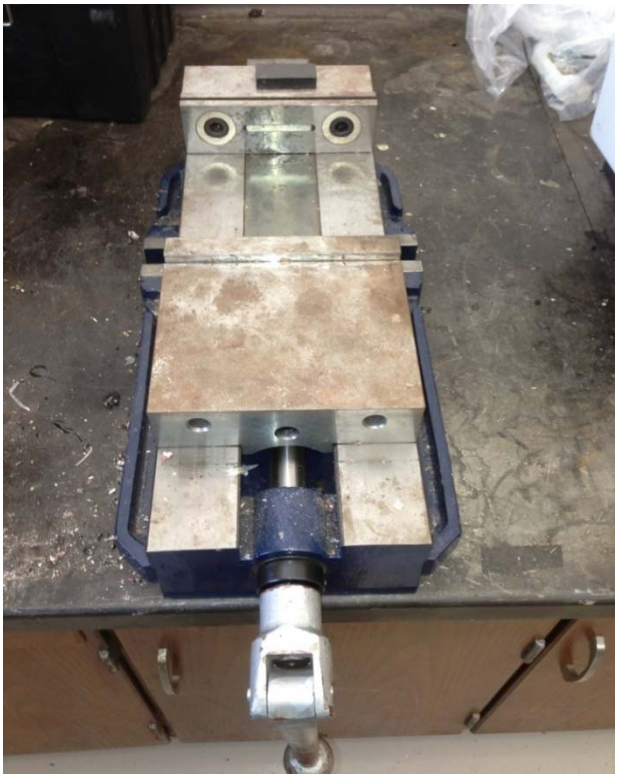

Figure 14. Gluing jig

Figure 15 shows that four pairs of Linear Variable Displacement Transducers (LVDTs) are glued on the four sides of the specimen to measure the vertical displacement of each side. They can measure the strain at the bottom, surface and center of the specimen during the test. This mechanical test is a non-destructive test which means there is even no micro cracking inside the specimen, after several dummy tests to estimate the maximum strain for a nondestructive test, 60 microstrains is adopted for this test. 10˚C and 20˚C are the test temperatures in order to show the relationship between temperature and modulus for field cores. It takes about two hours to have the specimen reach the required temperature in the chamber each time.

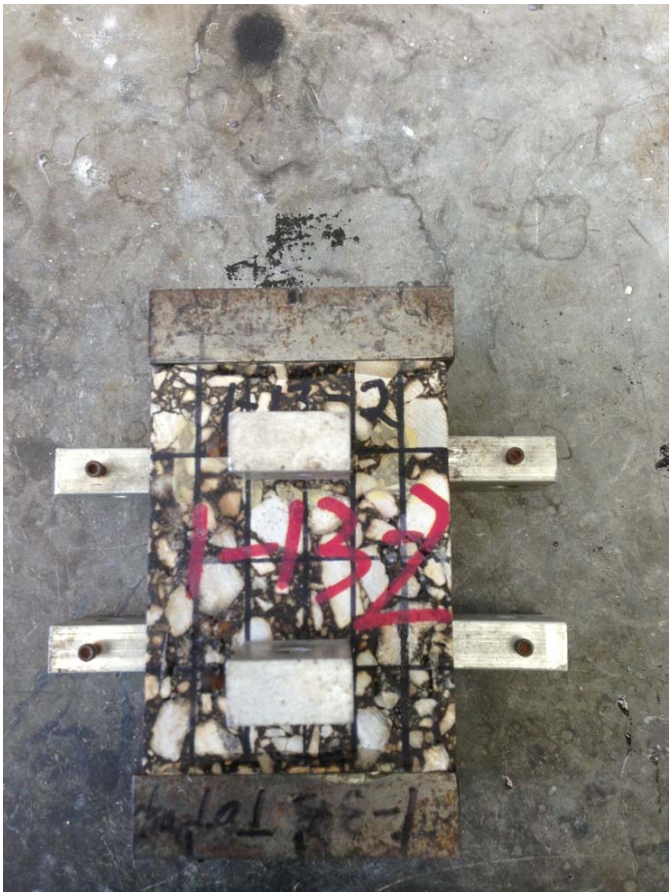

Figure 15. Specimen glued with LVDTs

The test temperatures are set on the MTS machine. 10˚C is the first test temperature, it takes four hours to start the machine and reach this temperature after the chamber was closed (see Figure 16). The feedback frequency of this MTS machine is 20HZ. Sometimes tests can be run at 30˚C when the specimen is aged enough otherwise it would take only a few seconds to reach the maximum strain which is 60 mircostrains in this test. Because of limited data from the test at 30˚C, most of the results at this temperature cannot be analyzed effectively.

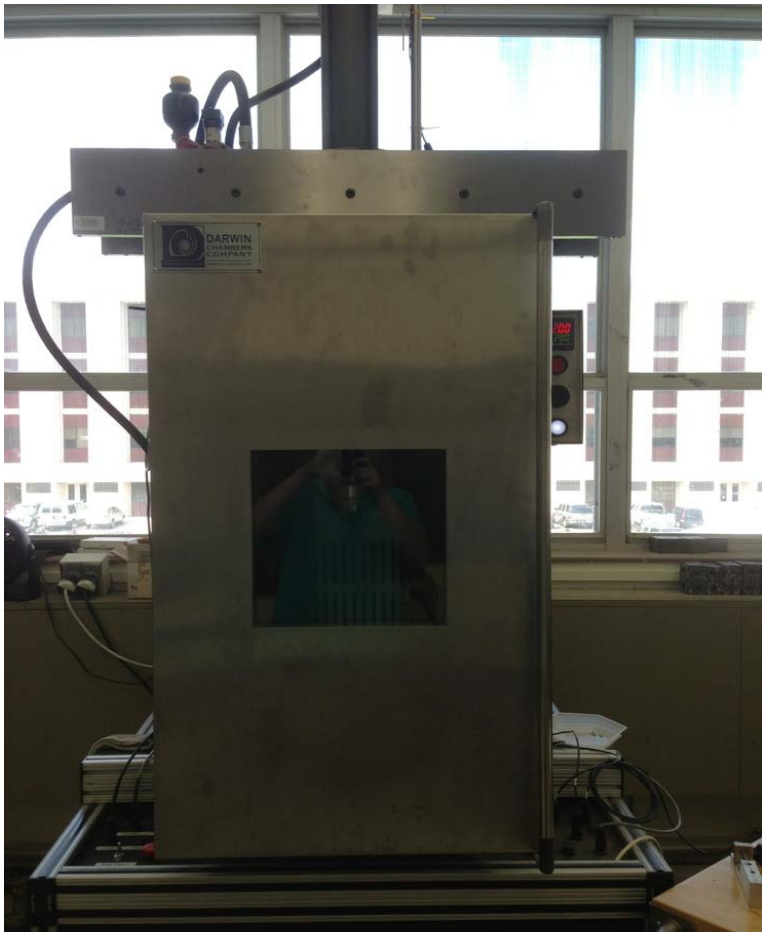

Figure 16. MTS machine with chamber closed

Before the test, the specimens and screw drivers were put into the chamber to have them reach the test temperature to ensure that the temperature of these specimens was the same as the test temperature in the chamber so there is no temperature difference between the specimen and screw drivers to avoid unexpected cracking (see Figure 17).

Figure 17. MTS machine with chamber opened

The chamber is closed during the test, dowel bar inside the chamber is used to pull the specimen in the vertical direction, and the other end of the specimen is fixed to a ball joint at the bottom of the MTS machine. The test automatically stops when the maximum strain is reached. The results of vertical displacement versus time of every side of the specimen are recorded in the computer.

3.2. Test Theory

Strain is assumed to be linear from the surface of the rectangular specimen to the bottom of it. A power function is also used to describe the modulus change from top to bottom.

$$E(z) = E_d + (E_0 - E_d)\left(\frac{d-z}{d}\right)^n \tag{7}$$

$$\varepsilon(z) = \varepsilon_0 + \frac{(\varepsilon_d - \varepsilon_0)}{d} \tag{8}$$

where $E(z)$=modulus at depth z, E_d= modulus at the bottom, E_0=modulus at the surface, n=model parameter which shows the shape of the modulus gradient, d = thickness of the specimen. $\varepsilon(z)$ and $\sigma(z)$ are the strain and stress at the depth, z. ε_d and ε_0 are strains at the bottom and surface of the layer, respectively.

$$\sigma(z) = E(z)\varepsilon(z) \tag{9}$$

$$\sigma(z) = \varepsilon_0 E_d + \frac{\varepsilon_d - \varepsilon_0}{d} E_d z + \varepsilon_0 (E_0 - E_d)(\frac{d-z}{d})^n + \frac{\varepsilon_d - \varepsilon_0}{d}(E_0 - E_d)(\frac{d-z}{d})^n z \tag{10}$$

The force is shown below where b is the thickness of the specimen,

$$P = b\int_{z=0}^{z=d} \sigma(z)dz \tag{11}$$

$$P = b\varepsilon_0 E_d d + b(\varepsilon_d - \varepsilon_0)E_d \frac{d}{2} + \frac{b\varepsilon_0 (E_0 - E_d)d}{n+1} + \frac{b(\varepsilon_d - \varepsilon_0)(E_0 - E_d)d}{(n+1)(n+2)} \tag{12}$$

Take the Laplace Transform of both sides:

$$\overline{P}(s) = s\overline{E}_d(s)\left[\overline{\varepsilon}_0(s)\left(1-\frac{1}{2}-\frac{1}{n+1}+\frac{1}{(n+1)(n+2)}\right)+\overline{\varepsilon}_d(s)\left(\frac{1}{2}-\frac{1}{(n+1)(n+2)}\right)\right]bd + s\overline{E}_0(s)\left[\overline{\varepsilon}_0(s)\left(\frac{1}{n+1}-\frac{1}{(n+1)(n+2)}\right)+\overline{\varepsilon}_d(s)\left(\frac{1}{(n+1)(n+2)}\right)\right]bd \quad (13)$$

Assume that

$$sE_0(s) = ksE_d(s) \quad (14)$$

where k is a constant and k >1, which means the modulus at the surface is k times larger than the modulus at the bottom. The above equation becomes:

$$s\overline{E}_d(s) = \frac{\overline{P}(s)}{bd\left\{\overline{\varepsilon}_0(s)\left[\frac{1}{2}+\frac{k-1}{n+2}\right]+\overline{\varepsilon}_d(s)\left[\frac{1}{2}+\frac{k-1}{(n+1)(n+2)}\right]\right\}} \quad (15)$$

where $\overline{\varepsilon}_0(s)$ is the Laplace Transform of the strain at the pavement surface with time, $\overline{P}(s)$ is the Laplace Transform of load with time, $\overline{\varepsilon}_d(s)$ is the Laplace Transform of the strain at the bottom of the pavement surface with time.

$$P = bd[E_d\varepsilon_0 + \frac{(\varepsilon_d-\varepsilon_0)E_d}{2} + \frac{\varepsilon_0(E_0-E_d)}{(n+1)} + \frac{(\varepsilon_d-\varepsilon_0)(E_0-E_d)}{(n+1)(n+2)(n+3)} \quad (16)$$

If $\bar{z}=\frac{d}{2}$,

$$P = 2bd[E_d\frac{\varepsilon_0}{2} + \frac{(\varepsilon_d-\varepsilon_0)E_d}{3} + \frac{\varepsilon_0(E_0-E_d)}{(n+1)(n+2)} - 4\frac{(\varepsilon_d-\varepsilon_0)(E_0-E_d)}{(n+1)(n+2)(n+3)} \quad (17)$$

The other expression for P is

$$P = bd[E_d\varepsilon_0 + \frac{(\varepsilon_d-\varepsilon_0)E_d}{2} + \frac{\varepsilon_0(E_0-E_d)}{(n+1)} + \frac{(\varepsilon_d-\varepsilon_0)(E_0-E_d)}{(n+1)(n+2)(n+3)} \quad (18)$$

Setting the two P equations equal gives

$$\frac{1-n}{(n+1)(n+2)} = \frac{1}{(n+1)(n+2)} \quad \Rightarrow \quad n = 0$$

n cannot be 0, because if n=0, there is no modulus change from surface to bottom which is impossible.

The strain amplitude at the surface, $\Delta\bar{\varepsilon}_0$ is related to the strain amplitude of the bottom of the surface layer, $\Delta\bar{\varepsilon}_d$, is as follows.

$$\frac{\Delta\bar{\varepsilon}_0(s)}{\Delta\bar{\varepsilon}_d(s)} = \frac{1}{k}.\frac{\bar{\varepsilon}_0(s).r_0 + \bar{\varepsilon}_d(s).r_d}{\bar{\varepsilon}_0(s).(t_0 - r_0) + \bar{\varepsilon}_d(s).(t_d - r_d)} \tag{19}$$

The ratio of the strain amplitude at the center $\Delta\bar{\varepsilon}_c$ to the strain amplitude at the bottom of the surface layer, $\Delta\bar{\varepsilon}_d$, is as follows.

$$\frac{\Delta\bar{\varepsilon}_c(s)}{\Delta\bar{\varepsilon}_d(s)} = \frac{2^n}{2^n - 1 + k}.\frac{\bar{\varepsilon}_0(s).(\frac{t_0}{2} - r_0) + \bar{\varepsilon}_d(s).(\frac{t_d}{2} - r_d)}{\bar{\varepsilon}_0(s).(t_0 - r_0) + \bar{\varepsilon}_d(s).(t_d - r_d)} \tag{20}$$

where $\Delta\bar{\varepsilon}_d(s)$, $\Delta\bar{\varepsilon}_c(s)$ and $\Delta\bar{\varepsilon}_0(s)$ = bottom, center, and top oscillating strain amplitudes, respectively.

The moment that is caused by the eccentricity of the load is

$$\bar{M}(s) = \bar{P}(s)\bar{e}(s) \tag{21}$$

The eccentricity, e, is

$$e = \frac{d}{2} - \bar{z} \tag{22}$$

$$\bar{M}(s) = s\bar{E}_d(s) \cdot bd^2 \left(\varepsilon_0(s)\left(\frac{t_0 - r_0}{2}\right) + \varepsilon_d(s)\left(\frac{t_d - r_d}{2}\right)\right) \tag{23}$$

where $r_0 = \frac{1}{6} - \frac{n(k+1)+5k+1}{(n+1)(n+2)(n+3)}$, $r_d = \frac{1}{3} - \frac{2(k-1)}{(n+1)(n+2)(n+3)}$, $t_0 = \frac{1}{2} + \frac{(k-1)}{(n+2)}$,

$t_d = \frac{1}{2} + \frac{(k-1)}{(n+1)(n+2)}$

$$\sigma = \frac{Mc}{I}$$

$$E_0\varepsilon_0 = \sigma_0 = \frac{M\bar{Z}}{I_0}$$

$$E_d\varepsilon_d = \sigma_d = \frac{M(d-\bar{Z})}{I_d}$$

where I is the moment of inertia. Equations 24, 25 and 26 are strain amplitude values at the surface, bottom and center of the specimen, respectively.

$$\bar{\varepsilon}_0(s) = \frac{6}{k}\left[\frac{\overline{[\varepsilon_0}(s)(r_0) + \overline{\varepsilon_d}(s)(r_d)}{\overline{\varepsilon_0}(s)(t_0) + \overline{\varepsilon_d}(s)(t_d)}\right]\left[\overline{\varepsilon_0}(s)(t_0 - r_0) + \overline{\varepsilon_d}(t_d - r_0)\right] \tag{24}$$

$$\bar{\varepsilon}_d(s) = 6\left[\frac{\overline{[\varepsilon_0}(s)(t_0 - r_0) + \overline{\varepsilon_d}(s)(t_d - r_d)]^2}{\overline{\varepsilon_0}(s)(t_0) + \overline{\varepsilon_d}(s)(t_d)}\right] \tag{25}$$

$$\bar{\varepsilon}_c(s) = \frac{6 \times 2^n}{(2^n - 1 + k)}\left[\frac{\overline{[\varepsilon_0}(s)(t_0 - r_0) + \overline{\varepsilon_d}(s)(t_d - r_d)]^2}{\overline{\varepsilon_0}(s)(t_0) + \overline{\varepsilon_d}(s)(t_d)}\right] \tag{26}$$

Equations 24, 25 and 26 are used to calculate *n* and *k*. The values of $\frac{\bar{\varepsilon}_0(s)}{\bar{\varepsilon}_d(s)}$ and $\frac{\bar{\varepsilon}_c(s)}{\bar{\varepsilon}_d(s)}$ can be found after analyzing the data with excel spreadsheets. Then caps can solve for *n* and *k* in the simultaneous equations above. The *n* values are used in Equation 7 for the final calculation and figure plotting.

3.3. Data Analysis

Measured vertical strains (microstrain), time and force are calculated using the equation:

$$\varepsilon = \frac{l - L}{L} \times 10^6, T = \Delta T = T_n - T_0, F = F_n - F_0 \tag{27}$$

Fitted force and vertical strains (microstrain) are fitted using the equations:

$$F(t) = a \times \left(1 - e^{bt}\right) + c \tag{28}$$

$$\varepsilon(t) = a \times \left(1 - e^{bt}\right) + c \tag{29}$$

where a , b and c are fitted parameters of the equation.

Least square method and solver function are used to get a, b and c. Typical oscillating strain and force at the center of the specimen are shown in Figure 18 in Figure 19.

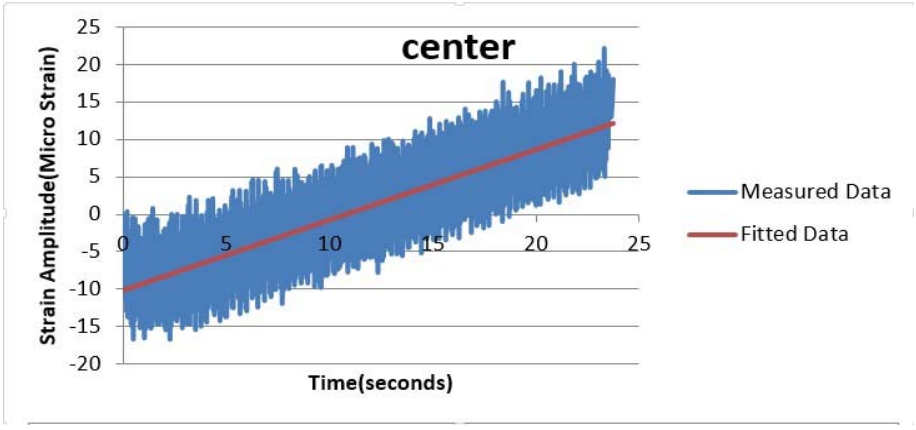

Figure 18. Fitted data and measured data of strain amplitude at the center of the sample

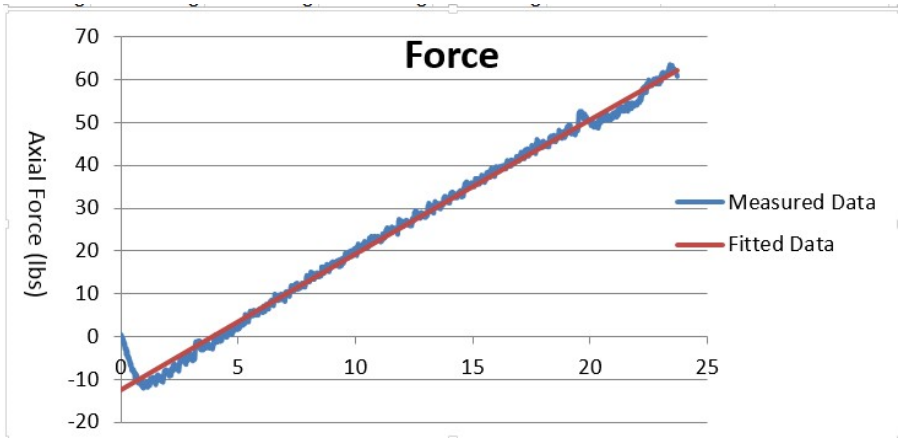

Figure 19. Fitted data and measured data of force

The difference between measured force or strain and fitted force or strain is calculated as delta force or strain. The result is a band the width of which is the oscillation amplitude.

The test time period for analyzing begins at 2 seconds and ends at 12 seconds to ensure it a continuous procedure and having enough data. The sum total and number of the strains which exceed the estimated maximum and minimum are recorded for the center, bottom and surface. Also the average of these numbers are calculated.

$$\Delta\bar{\varepsilon}(s)=\frac{2}{s}(a_1+a_2)-\frac{2a_2 s}{s^2+\omega^2} \tag{30}$$

where $a_1=\overline{\min}$, $a_2=\dfrac{\overline{\max}-\overline{\min}}{2}$, $\omega=\dfrac{2\pi}{0.7}$ and $S=20\times 2\pi$

3.4. Results

The field cores from Arizona, Yellowstone National Park and Texas FM 973 have been tested and analyzed using the method stated above. The values of the model parameters *n, k*, surface and bottom modulus were obtained after analyzing the data from the test. Several figures were drawn using the modulus gradient model. The results of all the parameters in this model are stated in Table 5, Table 6 and Table 7.

Table 5. Analysis results of stiffness gradient for Arizona field cores

Sample ID	*n*	*k*	Surface Modulus (MPa)	Bottom Modulus (MPa)	Temperature (°C)
AZ1-1A	4.57	1.37	4636	3386	10
AZ1-2A	4.14	2.62	5274	2009	10
AZ1-3A	4.57	2.97	7851	2640	10
AZ1-4A	4.29	2.86	5565	1943	10
AZ1-1A	1.71	3.52	4508	1281	10
AZ1-2A	3.69	1.45	3180	2185	10
AZ1-3A	4.95	1.67	5097	3056	10
AZ1-4A	3.46	1.91	7736	4057	10
AZ1-1A	4.9	1.42	6729	4737	20
AZ1-2A	3.18	1.55	6930	4481	20
AZ1-3A	4.39	3.24	13114	4047	20
AZ1-4A	3.62	1.99	8597	4324	20
AZ1-1A	3.51	1.82	7095	3895	20
AZ1-2A	4.11	2.91	11449	3938	20
AZ1-3A	2.31	1.42	4861	3423	20
AZ1-4A	5.19	1.36	9620	7054	20

Table 6. Analysis results of stiffness gradient for Yellowstone park field cores

Sample ID	*n*	*k*	Surface Modulus (MPa)	Bottom Modulus (MPa)	Temperature (°C)
1-3B-Top-WP	4.28	1.70	3761	2214	10
1-3B-Top-S	4.90	1.89	3278	1731	10
1-3B-Bot-WP	4.90	1.35	2509	1864	10
1-3B-Bot-S	4.93	1.65	2221	1343	10
1-2B-Top-WP	4.08	2.27	4710	2077	10
1-2B-Top-S	4.94	2.09	4486	2146	10
1-2B-Bot-WP	4.11	1.76	2578	1467	10
1-2B-Bot-S	3.92	1.64	2611	1592	10
1-3B-Top-WP	4.10	2.05	2827	1378	20
1-3B-Top-S	4.21	2.34	2385	1017	20
1-3B-Bot-WP	3.80	1.64	1689	1033	20
1-3B-Bot-S	4.34	1.52	1454	958	20
1-2B-Top-WP	4.09	2.01	3062	1526	20
1-2B-Top-S	4.13	2.31	3235	1397	20
1-2B-Bot-WP	3.74	1.66	1644	989	20
1-2B-Bot-S	4.15	1.83	1859	1014	20

Table 7. Analysis results of stiffness gradient for Texas field cores

Sample ID	*n*	*k*	Surface Modulus (MPa)	Bottom Modulus (MPa)	Temperature (°C)
1-13-1	4.98	1.36	3349	2471	10
1-20-1	4.77	1.51	4271	2824	10
1-26-1	4.93	1.44	3836	2660	10
1-27-1	3.78	1.43	3299	2314	10
1-28-1	3.53	1.30	3357	2584	10
S1-2	3.93	1.70	6235	3677	10
S1-13	3.51	1.80	5528	3077	10
S1-20-1	3.38	1.72	6198	3611	10
S1-24	3.71	1.65	5727	3475	10
7-5-1	5.57	1.18	2917	2463	10
7-15-1	5.36	1.35	3268	2425	10
7-16-1	5.12	1.29	2898	2243	10
7-21-1	4.75	1.22	2775	2282	10
7-24-1	4.93	1.25	3287	2634	10
S7-5	4.30	1.88	5310	2828	10
S7-12	3.96	1.61	5580	3456	10
S7-15	4.69	1.95	6411	3292	10
S7-16	4.15	1.75	5348	3057	10
8-4-1	4.86	1.22	2440	1993	10
8-8-1	4.94	1.31	2235	1708	10
8-12-1	4.15	1.37	2730	2000	10
8-18-1	5.03	1.38	2102	1520	10
8-20-1	4.12	1.37	2824	2065	10
8-24-1	4.12	1.28	2348	1833	10
S8-4	4.73	2.12	4626	2182	10
S8-8	4.09	2.02	5122	2539	10
S8-12	4.91	1.76	5209	2966	10
S8-18	5.02	1.84	4788	2608	10
1-13-1	4.1	1.38	3101	2246	20
1-26-1	4.89	1.53	3073	2005	20
1-27-1	3.99	1.31	2639	2019	20
1-28-1	4.93	1.5	2460	1633	20

Table 7 (*Continued*)

Sample ID	*n*	*k*	Surface Modulus (MPa)	Bottom Modulus (MPa)	Temperature (°C)
S1-2	4.15	1.77	5202	2935	20
S1-13	3.85	1.67	4740	2832	20
S1-24	5.36	1.65	4561	2756	20
7-16-1	4.93	1.39	2115	1530	20
7-21-1	4.1	1.22	1743	1419	20
S7-5	5	1.84	4437	2880	20
S7-12	4.07	1.76	4885	2784	20
S7-15	4.91	2.02	4968	2460	20
S7-16	4.1	1.64	4313	2618	20
8-8-1	4.93	1.38	1805	1309	20
8-12-1	4.76	1.27	2219	1743	20
8-18-1	4.02	1.41	2122	1502	20
S8-12	4.23	1.84	3907	2129	20
S8-18	5.19	1.92	3576	1867	20

Figure 20 shows that there is a wide range of surface modulus in this pavement which ranges from 3180 MPa to 13114 MPa in this Arizona pavement. This phenomenon proves that it is not easy to mimic the actual condition of pavement in the lab as stated previously in the introduction. A depth of 0.8 inch is an estimated depth of severe aging, below 0.8 inch, the aging goes through deeply into pavement. The aging is severe in this pavement because wherever the surface modulus is higher than 10000 MPa, extensive cracking may emerge in the near future so some maintenances are necessary. It is interesting to compare Figure 20 with the second figure found on page 43 which can show that Arizona field cores are more aged than the Yellowstone National Park cores because they are 108 months aged while the cores from Yellowstone National

Park are 48 months aged. In addition, the modulus in the wheel path of the pavement is larger than which in the shoulder of the pavement.

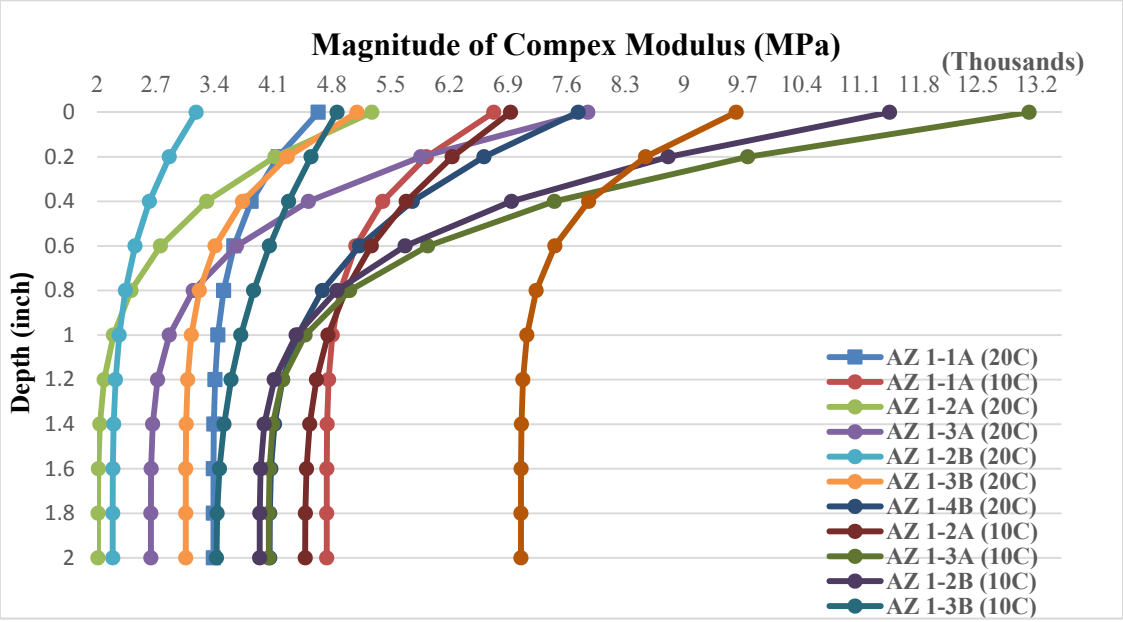

Figure 20. The stiffness gradient curve of Arizona at 10°C and 20°C

Figures 21 and 22 show test results from Texas FM 973 that the modulus at 10˚C is higher than the modulus at 20˚C. For the same specimen, no matter what the test temperature is, *n* and *k* values don't vary very much. Figure 21 shows that that the bottom lift is weaker than the surface lift.

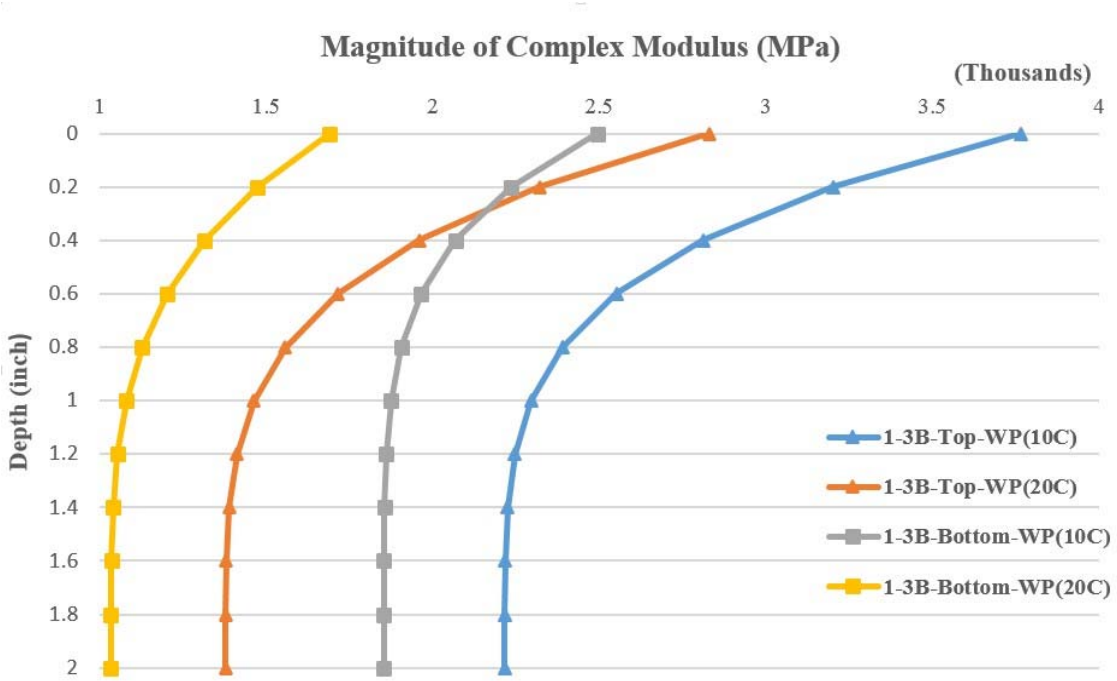

Figure 21. Comparison of top and bottom layers at 10˚C and 20˚C from Texas FM 973

Figure 22 and Figure 23 show that higher rate of aging in the wheel path than in the shoulder because of the traffic is higher in the wheel path than in the shoulder and as the temperature increases the modulus decreases as stated above.

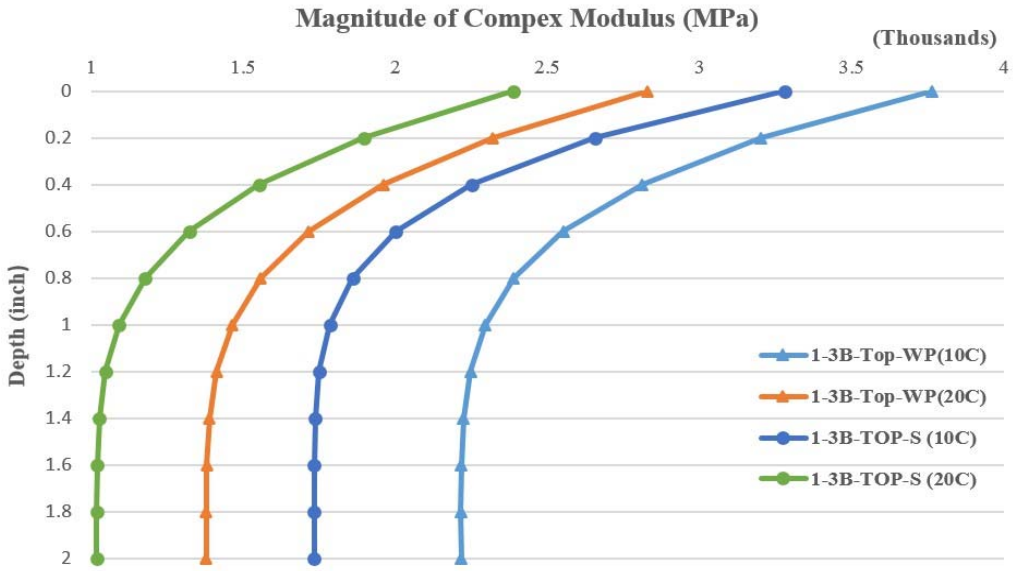

Figure 22. Comparison of different position at 10°C and 20°C from Texas FM 973 (WP-Wheel Path; S-Shoulder)

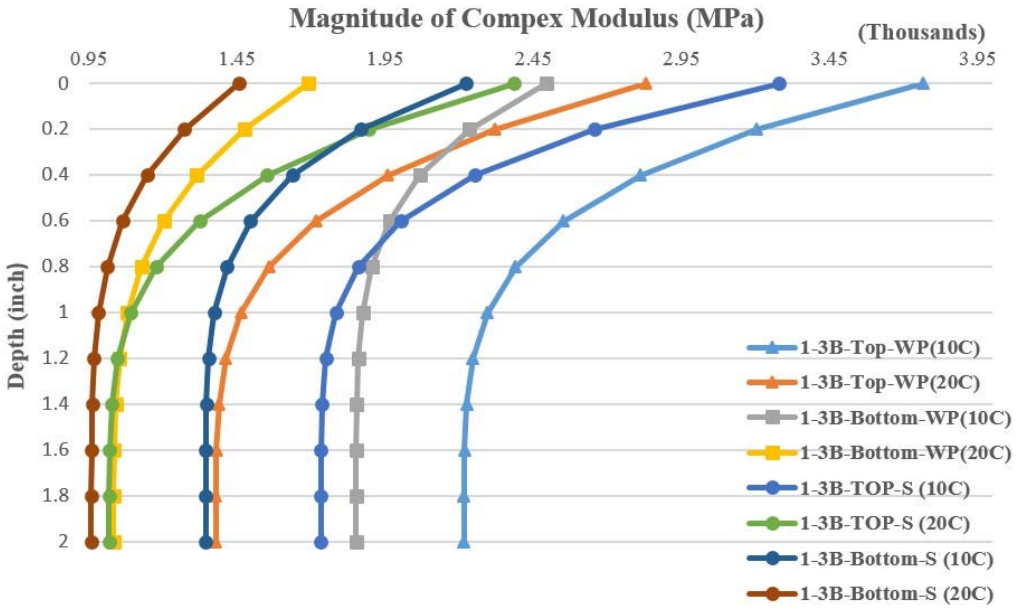

Figure 23. The stiffness gradient curve of Yellowstone National Park at 10°C and 20°C

For Texas field cores, the modulus of HMA (section 1) is higher than the modulus of foaming WMA (section 7) and the modulus of foaming WMA is higher than the modulus of Evotherm WMA (section 8) at the same aging time especially in the very early aging period. However, the increasing rate of section 8 is the highest and the increasing rate of section 7 is also higher than the increasing rate of section 1 if the aging time increases, the modulus of Evotherm and foaming sections will catch up with the modulus of the HMA. In conclusion, at the beginning of aging (pavement in use), more attention should be paid to Evotherm WMA than foaming WMA because they are weaker than HMA. After a long time use, maintenance should be conducted on all of these sections no matter what kind of pavement it is. Details are included in Table 8 as follows:

Table 8. Average modulus values and increase rate

Section Number	Section 1		Section 7		Section 8	
Location	Surface	Bottom	Surface	Bottom	Surface	Bottom
Average Modulus Value μ (1 Month aged)	3622.4	2570.6	3029	2409.4	2447.8	1825.2
Average Modulus Value μ (8 Month aged)	5922	3460	5662.25	3158.25	4936.25	2573.75
Increasing Rate (%)	63.4828	34.5989	86.9346	31.0804	101.661	41.0119

It can be shown in Figure 24 that the 8 months aged specimens have a severe aging depth of 1 inch from the surface, however, the 1 month aged specimens have a gentle curve which indicates that they are only aged in the first 0.3 inch depth.

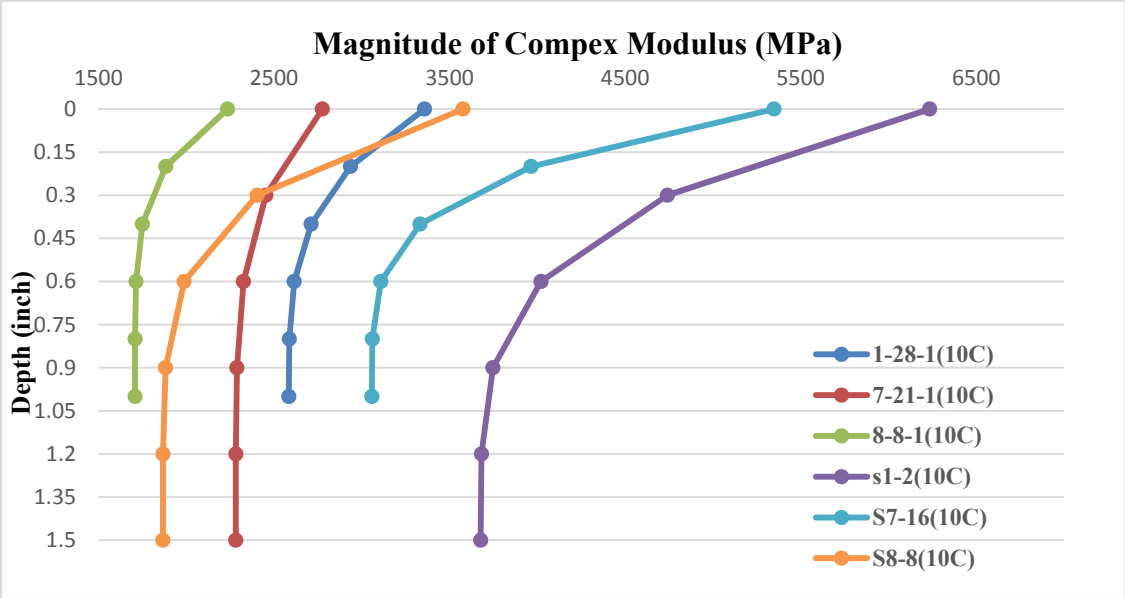

Figure 24. Stiffness gradient of Texas FM 973 (HMA, Foaming, Evo) at 10°C

There are three different layers collected from FM 973. According to the Pavement Management Information System (PMIS) in Texas (see Figure 25), this pavement has been renovated two times since 2005 and the condition scores have been returned to 100. It indicates that two overlays have been paved in 2005 and 2009. Each time the pavement surface has been highly aged and when the modulus of the surface layer has reached a significant level, a new overlay would be paved above. The results of Figure 26 can show when these two renovations were done because these layers are independent with each other. And for the second and third layers, they have been highly aged and it indicates that the aging can happen through the depth of each layer.

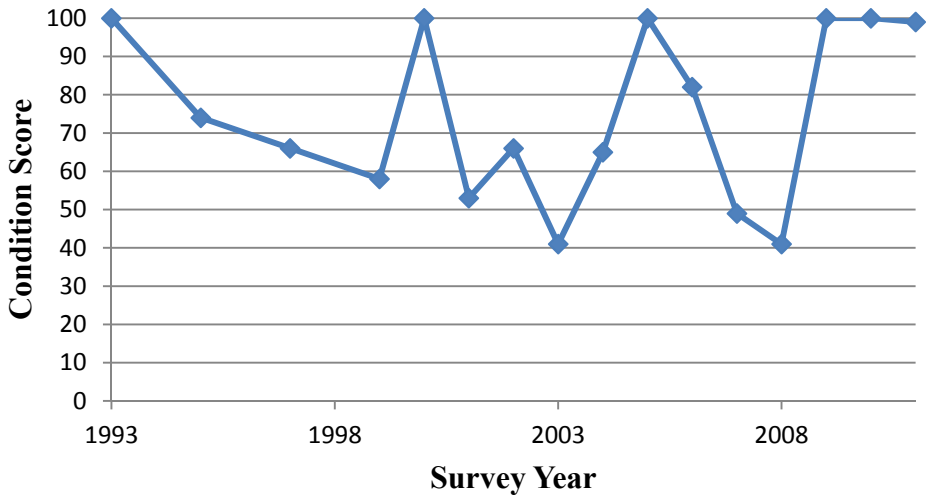

Figure 25. Pavement condition score versus survey year (PMIS)

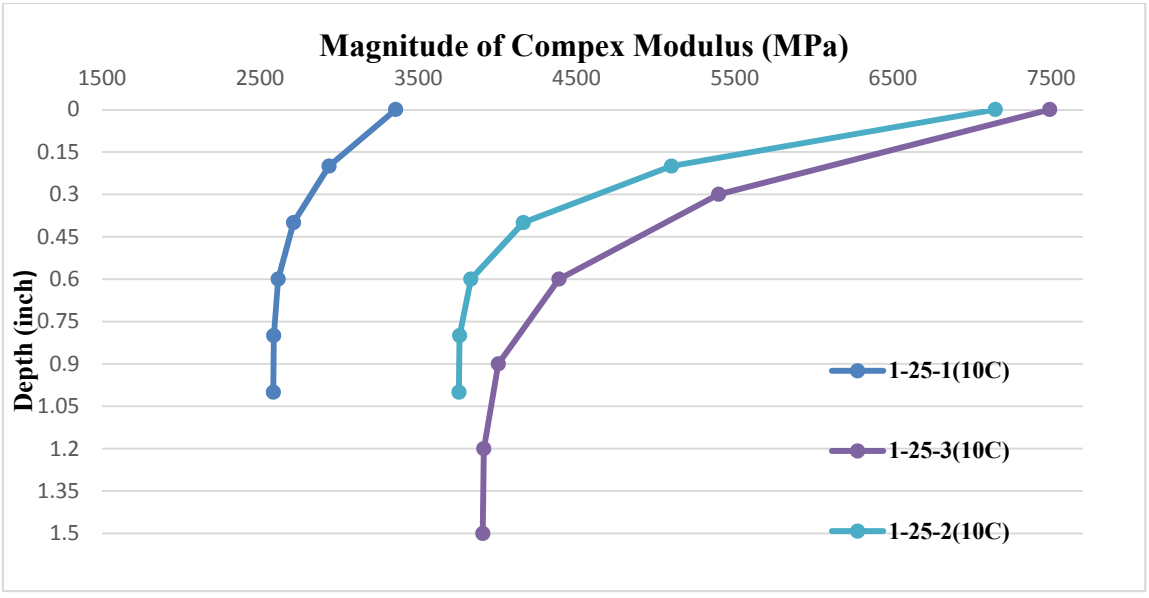

Figure 26. Cores from different layers of one specimen

4. THE MODELS DERIVED FROM MODULUS GRADIENT

Table 9, Table 10 and Table 11 show the statistical analysis for the results of HMA, Foaming WMA, Evotherm WMA samples respectively at 10˚C of 0/1 month aged.

Table 9. Statistical summary of HMA at 10˚C (1 month aged)

HMA	*n*	*k*	Modulus at Surface (MPa)	Modulus at Bottom (MPa)
μ	4.77	1.51	4271	2824
б	0.68	0.08	423.11	192.45
COV, %	14.26	5.23	9.90	6.81

Table 10. Statistical summary of Foaming at 10˚C (0 month aged)

Foaming	*n*	*k*	Modulus at Surface (MPa)	Modulus at Bottom (MPa)
μ	5.146	1.258	3029	2409.4
б	0.328	0.065	233.402	156.110
COV, %	6.369	5.194	7.710	6.479

Table 11. Statistical summary of Evotherm at 10˚C (0 month aged)

Evotherm	*n*	*k*	Modulus at Surface (MPa)	Modulus at Bottom (MPa)
μ	4.540	1.313	2405	1836.5
б	0.473	0.076	259.428	224.655
COV, %	10.41	5.815	10.787	12.233

Table 12, Table 13 and Table 14 show the statistical analysis for the results of HMA, Foaming WMA, Evotherm WMA samples respectively at 10˚C of 8/9 months aged.

Table 12. Statistical summary of HMA at 10˚C (9 months aged)

HMA	*n*	*k*	Modulus at Surface (MPa)	Modulus at Bottom (MPa)
μ	3.66	1.7	6216.5	3644
б	0.388	0.014	26.163	46.670
COV, %	10.640	0.827	0.421	1.281

Table 13. Statistical summary of Foaming at 10˚C (8 months aged)

Foaming	*n*	*k*	Modulus at Surface (MPa)	Modulus at Bottom (MPa)
μ	4.965	1.8	4998.5	2787
б	0.077	0.057	297.692	253.144
COV, %	1.567	3.143	5.956	9.083

Table 14. Statistical summary of Evotherm at 10˚C (8 months aged)

Evotherm	*n*	*k*	Modulus at Surface (MPa)	Modulus at Bottom (MPa)
μ	4.137	1.75	5412.67	3113.67
б	0.170	0.135	146.16	317.82
COV, %	4.120	7.731	2.700	10.207

4.1. Base Modulus Aging Model

The average bottom modulus of Texas field cores at 10 °C is plotted against the aging time for three different asphalt mixtures: hot asphalt mix (HMA), foamed warm asphalt mix (FWMA), WMA with Evotherm additive (Evotherm), as shown in Figure 27. The curves are simulated by the following model:

$$E_b(t) = E_1(t+1)^{\kappa} \tag{31}$$

where $E_b(t)$ is the aged modulus at 1.5 inches depth; t is the aging time in months; E_1 and κ are base modulus aging model coefficients. Table 15 shows the base modulus aging model coefficients for HMA, FWMA, and Evotherm, respectively.

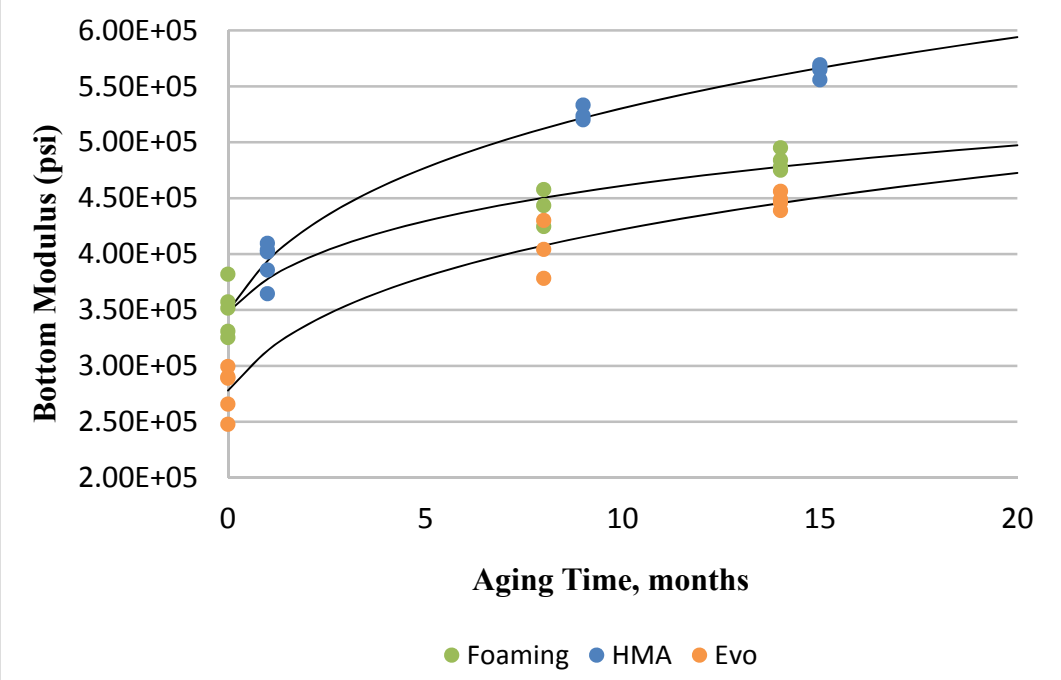

Figure 27. Bottom modulus versus aging time for different mixtures

Table 15. Base modulus aging model coefficients for different mixtures

Type of Mixture	Base Modulus Aging Model Coefficients		R^2 Values
	E_1 (psi)	κ	
HMA	3.489×10^5	0.1748	0.9785
FWMA	3.482×10^5	0.1171	0.9229
Evotherm	2.779×10^5	0.1744	0.9539

The number of load cycles of a standard load to reach the fatigue life of a pavement is N_f, it is proportional to

$$N_f \propto \left[\frac{(\Delta G)^{1+n'} E}{\sqrt{\%air}}\right](SF_n)\left[\frac{1}{\gamma d^{\frac{2(2n'-3)}{n'}}}\right] \tag{32}$$

where N_f = fatigue life, yrs.

% air= percent air in the mix

γ= shear strain

d= thickness of asphalt layer

E= modulus of asphalt layer

ΔG = bond energy between binder and asphalt

SF_n = shift factor due to healing

n' =fracture exponent

The number of load cycles of a standard load to reach the fatigue life of a pavement is inversely proportional to the DSR function, i.e., adjusted for the healing effect

$$\frac{1}{DSRf_n} \propto \frac{N_f}{SF_n} \tag{33}$$

First, find a calibration constant (C_{Nf}) for the mixture-based fatigue life

$$t = \left[\frac{N_f}{SF_n}\right] = \left(C_{nf}\right)\frac{\left(\Delta G\right)^{1+n'} E}{\sqrt{\%air}} \tag{34}$$

Second, find a calibration constant (C_D) for the DSR function-based fatigue life

$$t = \left[\frac{N_f}{SF_n}\right] = \frac{\left(C_D\right)}{DSRf_n} \tag{35}$$

Then set the two expressions equal to each other to get

$$\begin{aligned} \frac{C_D}{DSRf_n} &= (C_{Nf})\frac{(\Delta G)^{1+n'} E}{\sqrt{\%air}} \\ DSRf_n &= \frac{(C_D)\sqrt{\%air}}{(C_{Nf})(\Delta G)^{1+n'} E} \end{aligned} \tag{36}$$

where ΔG = wet adhesive bond energy

E = asphalt modulus

n' = fatigue exponent

%air= decimal air void content of the asphalt mixture

The target fatigue lives of pavements carrying heavy traffic as determined in the TTI Project 0-6386 Report in the different climate/soils zones in Texas are as follows (for the medium level rehab treatment) in years.

$$\frac{N_f}{SF_n} = \frac{wet\ freeze}{11yr} \quad \frac{wet-no\ freeze}{22yr} \quad \frac{dry-freeze}{87yr} \quad \frac{dry-no\ freeze}{18yr} \tag{37}$$

Use these lives to determine C_{Nf} for each climate/soils zone. Also, use these same lives to determine the C_D for each climate/soil zone.

In calculating the calibration coefficients, C_D and C_{Nf}, use the customary units for all of the variables such as ΔG_{dry}, E and % air. DSR function at 15˚C, 0.005 rad/sec.

$$DSRfn = D_o \times t^{n_A} \tag{38}$$

Observed values of D_o and n_A are in Table 16.

Table 16. Values of D_o and n_A for different locations in Texas

Pavement Location	Climate/Soils Zone	ln [D_o] (D_o(MPa/sec))	n_A
Pharr, Texas	D-NF	-3.523	0.296
Amarillo, Texas	D-F	-4.000	0.295
Texas, 21	W-NF	-4.745	0.200

The asphalt mixture modulus, E, ages and the observed aging function for modulus on the FM 973 Project is

$$E\ (t,\ yrs)\ =\ E_1\ (1+12t)^{\kappa} \tag{39}$$

The value for E_1 and κ for the Hot Mix and Warm Mixes on the FM 973 Projects are in Table 17.

Table 17. E_1 and κ values for three mixtures

Mixture Type	E_1(Psi)	κ
Hot Mix	3.67×10^5	0.159
Foaming	3.50×10^5	0.117
Evotherm	2.66×10^5	0.189

The observed fatigue exponents with field cores tested in the overlay tester on cores from the FM 973 Project are in Table 18 (they were tested dry).

$$n' = 2.4 + n_{n'}t\ (yrs) \tag{40}$$

Table 18. $n_{n'}$ for three mixture types for three mixtures

Mixture Type	$n_{n'}$
Hot Mix	0.0135
Foaming	0.0115
Evotherm	0.0135

The observed fatigue exponents for laboratory moisture conditioning observed with full mixes on lab-compacted/lab-mixed samples were larger than for those that were laboratory aged are in Table 19.

Table 19. Parameters for three mixtures types

Mixture Type	Field aging $n_{n'}$	Moisture Conditioning Multipliers	Full-Mix Moisture $n_{n'}$
Hot Mix	0.0135	1.000×1.954	0.0264
Foaming	0.0115	0.662×3.31	0.0252
Evotherm	0.0135	0.754×2.39	0.0243

The values of $n_{n'}$ to use in determining the value of C_{Nf} are the moisture conditioned full mix values. The calculated dry adhesive bond energy should be raised to these powers multiplied by the target number of years of fatigue life for each climate/soils zone in determining the calibration coefficient. The relation between the DSR function and pavement fatigue life is stated in Table 20.

Table 20. Relation between the DSR function and pavement fatigue life

			WET-FR	WET-NOF	DRY-FR	DRY-NOF
DSR Functions MPa/sec	Hot Mix		2.13E-05	2.13E-05	2.13E-05	2.13E-05
	Warm Mix (EVO)		1.97E-05	1.97E-05	1.97E-05	1.97E-05
	Warm Mix(Foaming)		3.67E-05	3.67E-05	3.67E-05	3.67E-05
Maximum Allowable DSR Functions (Neat Binder) MPa/sec	D_0	HMA	2.04E-05	8.27E-05	0.00012	4.84E-05
	D_0	WMA(EVO)	2.65E-05	1.03E-04	1.48E-04	6.15E-05
	D_0	WMA(Foaming)	2.98E-05	1.08E-04	1.53E-04	6.58E-05
	$Log_{10}(D_0)$	HMA	-4.69032	-4.08241	-3.9208	-4.31495
	$Log_{10}(D_0)$	WMA(EVO)	-4.57647	-3.98528	-3.82903	-4.21109
	$Log_{10}(D_0)$	WMA(Foaming)	-4.52569	-3.96617	-3.81666	-4.18205

The climate zone in Texas is shown in Figure 28, zone 1 is the dry-freeze zone, zone 2 is the wet-no freeze zone, zone 3 is the wet-freeze zone, and zone 4 is the dry-no freeze zone.

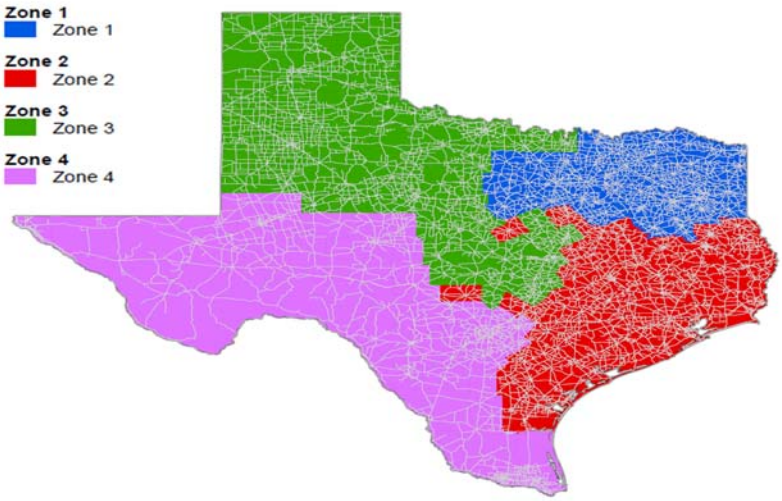

Figure 28. Climate/soils zones in Texas

4.2. Base Modulus Time-Temperature Shift Model

The Arizona, Yellowstone, and Texas field cores data are used to develop the time-temperature shift model as follows:

$$\ln a_T = \beta\left(T - T_0\right) \tag{41}$$

where a_T is the time-temperature shift factor, calculated by:

$$a_T = \frac{E_b(10°C)}{E_b(20°C)} \tag{42}$$

where $E_b(10°C)$ is the base modulus at 10°C and $E_b(20°C)$ is the base modulus at 20°C.

β is the time-temperature shift coefficient which are in Table 21.

T is the temperature and T_0 is reference temperature.

Figure 29 shows the plot of $\ln a_T$ versus the temperature, and Table 21 presents the values of β .

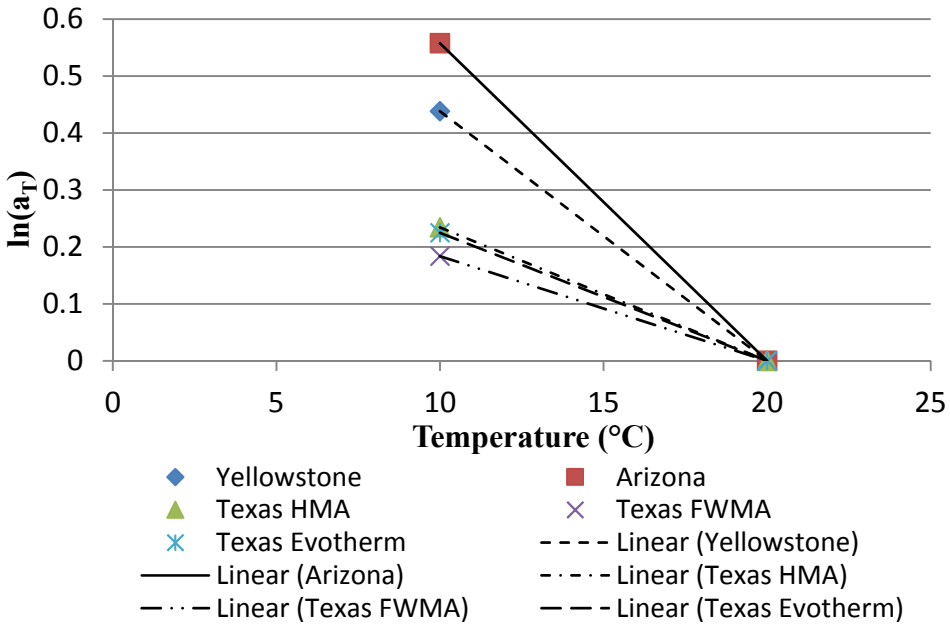

Figure 29. Plot of time-temperature shift factor versus temperature

Table 21. Value of β for different types of mixtures

Type of Mixture	β
Arizona	-0.0558
Yellowstone	-0.0438
Texas HMA	-0.0234
Texas FWMA	-0.0184
Texas Evotherm	-0.0225

4.3. Process Model of Relative Stiffness Ratio

The Arizona, Yellowstone, and Texas field cores data are used to develop time-temperature shift model as follows:

$$\ln k = k_0 - \frac{S}{T} \tag{43}$$

where k_0 is the intercept; $S$is the slope; and T is the absolute temperature. Figure 30 shows the plot of $\ln k$ versus T , and the values of k_0 and S are given in Table 22. In addition, the intercept and slope of the rate process model are plotted versus the solar radiation, which forms a nearly straight line as shown in Figure 31 and Figure 32, respectively. The value of solar radiation is obtained from Figure 33.

$\ln \bar{k}$ is calculated using the results below:

$\ln \bar{k}$ (Arizona, 10˚C) =0.675 $\ln \bar{k}$ (Arizona, 20˚C) =0.831

$\ln \bar{k}$ (Yellowstone, 10˚C) =0.584 $\ln \bar{k}$ (Yellowstone, 20˚C) =0.652

$\ln \bar{k}$ (Texas, 10˚C) =0.430 $\ln \bar{k}$ (Texas, 20˚C) =0.460

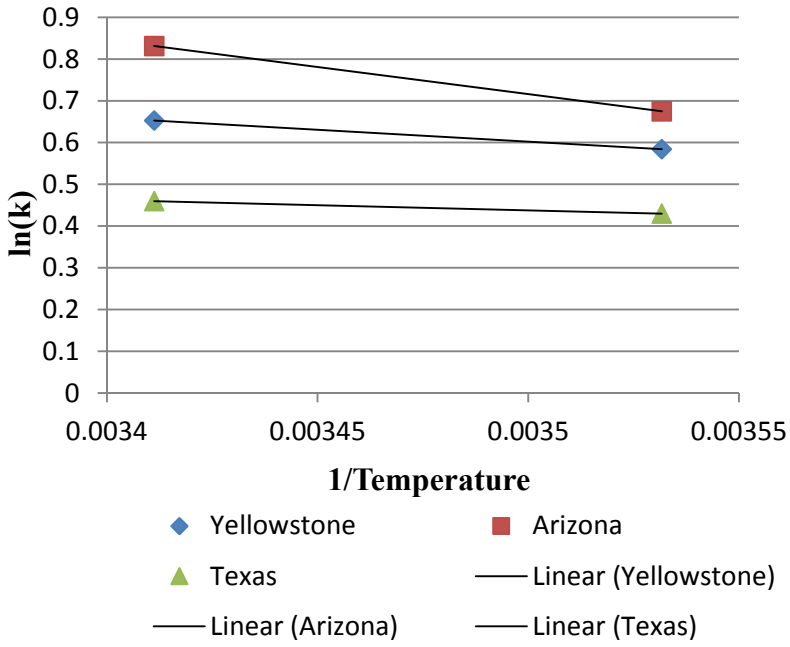

Figure 30. Plot of relative stiffness ratio versus absolute temperature

Table 22. Values of rate process model coefficients and solar radiation

Type of Mixture	k_0	s	Solar Radiation (MJ/m2-day)
Arizona	5.260	1298.4	26
Yellowstone	2.596	569.7	18
Texas	1.306	248.1	14

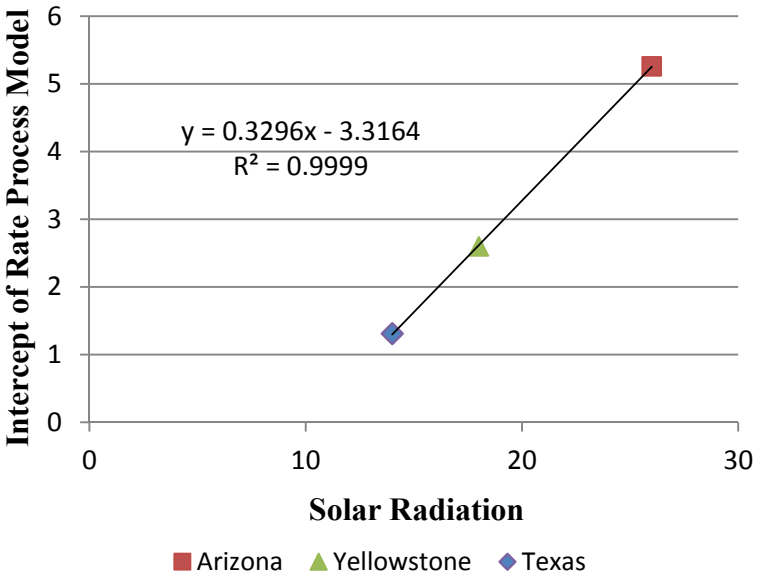

Figure 31. Plot of intercept of rate process model versus solar radiation

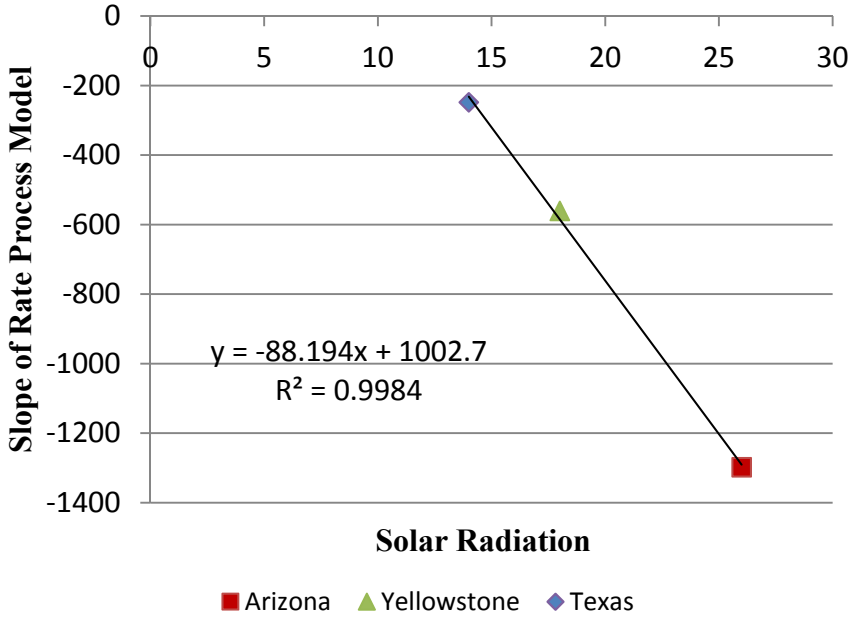

Figure 32. Plot of slope of rate process model versus solar radiation

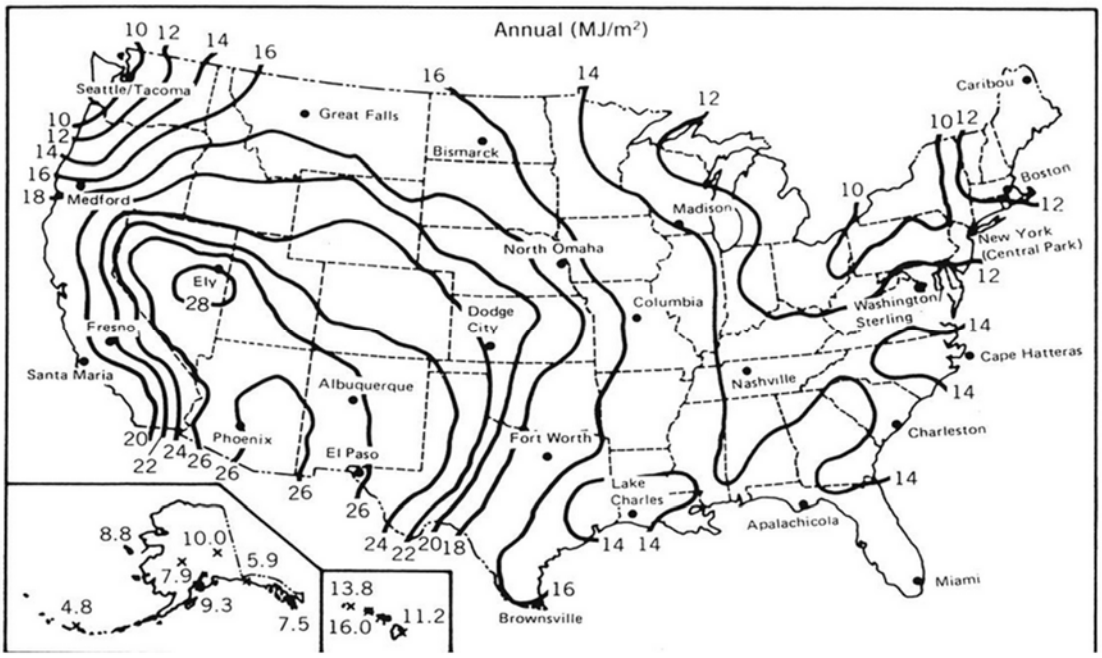

Figure 33. Annual average daily solar radiation in the United States (MJ/m^2) (Knapp and Stoffel, 1982)

An estimation of annual average daily solar radiation of certain places in the United States can be made from this figure (Knapp and Stoffel 1982). It is very interesting to show that the intercept and slope of the rate process model have an almost linear relationship with solar radiation. As a result, if the local solar radiation is known, the local *k* value can be estimated.

5. CONCLUSIONS, LIMITATIONS, AND FUTURE WORK

This section summarizes the main findings of the study, recommendations for future testing, some possible limitations, and future work of this study.

5.1. Detailed Conclusions

The viscoelastic properties of field cores are different from LMLC specimens which make field cores hard to be simulated. A mechanical test has been successfully developed and verified which is suitable for all field cores regardless of what kinds of material they consist of. The primary findings are listed below:

- The direct tension test is a quick, accurate, harmless to humans and nondestructive method which can be used to measure displacement of each side of asphalt concrete cores.
- Complex stiffness gradient of field cores and their profiles can be obtained after analyzing the data from the DT test.
- Several models have been established to evaluate and estimate current and future pavement conditions.
- Results can be utilized for improving existing models to better evaluate pavement conditions.

For complex stiffness gradient, it is easy to estimate the depth of highly aged asphalt mixtures. It can be used to help make a plan for applying an overlay or reconstruction. Compared with stiffness gradient figures of different asphalt mixtures, it

is clear to see which core has been more aged. From the tests conducted above, for the same aging time of 8 months, HMA cores have been aged more than FWMA cores which are more aged than Evotherm WMA. But after a longer period of aging time, these three types of asphalt pavement seem have been aged almost equally.
Models have been established to estimate the base modulus, time-temperature relationship, and relative stiffness ratio of the field cores in these pavement locations.

5.2. Limitations

- Based on the different complex modulus of specimens, a maximum control strain should be obtained from some dummy tests to avoid undesired cracking and it is not very easy to estimate. 60 microstrains is a suggested number for 0-8 months aged cores, 100 microstrains is a suggested number for over 5 years aged cores.
- Asphalt mixtures are temperature sensitive, 10˚C and 20˚C are the test temperatures but tests cannot be done at higher temperature, because the asphalt mixtures become too soft which makes the test time much shorter.
- The specimen should be aligned and glued between two steel end caps, and make sure the distance between two LVDTs are always 2 inches. It is not easy to follow this rule especially in the first few test preparations.

5.3. Future Work

- Even through some meaningful conclusions have been made, there is still some work that needs to be done such as simplifying calculations and controlling test fluctuations to make the analysis process a simple and straightforward method which can be easily converted into widespread use in the future.
- A higher test temperature is desired when it is applicable. Tests under three different temperatures are better to evaluate the viscoelastic properties of asphalt mixtures and easier to build master curves.
- Test results will be used in the Texas overlay tester which can measure the fracture and healing properties of asphalt mixtures.

REFERENCES

Bari, J., and Witczak, M. (2007). "New predictive models for viscosity and complex shear modulus of asphalt binders: For use with mechanistic-empirical pavement design guide." *Transportation Research Record*, 2001, 9-19.

Birgisson, B., Sholar, G., and Roque, R. (2005). "Evaluation of a predicted dynamic modulus for Florida mixtures." *Transportation Research Record*, 1929, 200-207.

Burr, B., Glover, C., Davison, R., and Bullin, J. (1993). "New apparatus and procedure for the extraction and recovery of asphalt binder from pavement mixtures." *Transportation Research Record* ,1391, 20-29.

Christensen, D., Pellinen, T., and Bonaquist, R. (2003). "Hirsch model for estimating the modulus of asphalt concrete." *Proc., Asphalt Paving Technology, March 10, 2003- March 12,2003.* Association of Asphalt Paving Technologist ,72, 97-121.

Clyne, T. R., Marasteanu, M.O., Li, X., Chadbourn, B., Engstrom, G., and Worel, B. (2004). "Determination of HMA modulus values for use in mechanistic-empirical pavement design." *Proc., 2nd International Conference on Accelerated Pavement Testing*, Minneapolis, Minnesota.

Collins-Garcia, H., Tia, M., Roque, R., and Choubane, B. (2000). "Alternative solvent for reducing health and environmental hazards in extracting aphalt." *Transportation Research Record*, 1712, 79-85.

Dongre, R., Myers, L., D'Angelo, J., Paugh, C., Gudimettla, J., Christensen, D., Heitzman, M., Page, G., Dukatz, E., and King, G. (2005). "Field evaluation of witczak and hirsch models for predicting dynamic modulus of hot-mix asphalt." *Proc.,Meeting of the Association of Asphalt Paving Technologists, March 7, 2005- March 9, 2005* Association of Asphalt Paving Technologist, 74, 381-442.

El-Badawy, S., Awed, A., and Bayomy, F. (2011). "Evaluation of the MEPDG dynamic modulus prediction models for asphalt concrete mixtures." *Proc., Transportation and Development Institute Congress 2011*, American Society of Civil Engineers (ASCE), 576-585.

Farrar, J. M., Harnsberger, P. M., and Kenneth, P. T. (2006). "Evaluation of oxidation in asphalt pavement test sections after four years of service." *Proc.,International Conference on Perpetual Pavement*, 1-17.

Fonseca, O. A., and Witczak, M. W. (1996). "Prediction methodology for the dynamic modulus of in-place aged asphalt mixtures." *Proc., Conference of the Association of Asphalt Paving Technologies: Asphalt Paving Technology*, *March 18, 1996 - March 20, 1996*, Assoc of Asphalt Paving Technologists, 532-572.

Huang, S.-C., and Grimes, W. (2010). "Influence of aging temperature on rheological and chemical properties of asphalt binders." *Transportation Research Record*, 2179, 39-48.

Knapp, C., and Stoffel, T. (1982). "Direct normal solar radiation data manual, long-term, monthly mean, daily totals for 235 national weather stations." Solar Energy Research Institute (SERI), Golden, Colorado, SERI/SP-281-1658.

Koohi, Y., Lawrence, J., Luo, R., and Lytton, R. (2012). "Complex stiffness gradient estimation of field-aged asphalt concrete layers using the direct tension test." *Journal of Materials in Civil Engineering*, 24(7), 832-841.

Masad, E., Jandhyala.K., Dasgupta, N., Somadevan, N., and Shashidhar. N. (2002). "Characterization of air void distribution in asphalt mixes using x-ray computed tomography." *Journal of Materials in Civil Engineering*, 14(2), 122-129.

Nazarian, S., and Alvarado, G. (2006). "Impact of temperature gradient on modulus of asphaltic concrete layers." *Journal of Materials in Civil Engineering*, 18(4), 492-499.

Shu, X., and Huang, B. (2008). "Dynamic modulus prediction of HMA mixtures based on the viscoelastic micromechanical model." *Journal of Materials in Civil Engineering*, 20(8), 530-538.

Tia, M., and Choubane, B. (2000). "Evaluation of an alternative solvent for extraction fo asphalt to reduce health hazards." *Summary of Final Report*, *December 2000*, *BB-881*, Florida Department of Transportation.

Woo, J., Chowdhury, A., and Glover, C. (2008). "Field aging of unmodified asphalt binder in three Texas long-term performance pavements." *Transportation Research Record,* 2051, 15-22.